

arXiv:q-bio/0607041v1 [q-bio.TO] 23 Jul 2006

# Amplitude equation approach to spatiotemporal dynamics of cardiac alternans

Blas Echebarria

*Departament de Física Aplicada, Universitat Politècnica de Catalunya, Barcelona, Spain.*

Alain Karma

*Department of Physics and Center for Interdisciplinary Research on Complex Systems,  
Northeastern University, Boston, MA 02115.*

(Dated: May 22, 2006)

## Abstract

Amplitude equations are derived that describe the spatiotemporal dynamics of cardiac alternans during periodic pacing of one- [B. Echebarria and A. Karma, *Phys. Rev. Lett.* **88**, 208101 (2002)] and two-dimensional homogeneous tissue and one-dimensional anatomical reentry in a ring of homogeneous tissue. These equations provide a simple physical understanding of arrhythmogenic patterns of period-doubling oscillations of action potential duration with a spatially varying phase and amplitude as well as explicit quantitative predictions that can be compared to ionic model simulations or experiments. The form of the equations is expected to be valid for a large class of ionic models but the coefficients are only derived analytically for a two-variable ionic model and calculated numerically for the original Noble model of Purkinje fiber action potential. In paced tissue, the main result is the existence of a linear instability that produces a periodic pattern of discordant alternans. The wavelength of this pattern, equal to twice the spacing between nodes separating out-of-phase regions of alternans, is shown to depend on three fundamental lengthscales that are determined by the strength of cell-to-cell coupling, conduction velocity restitution and, more generally, memory effects. Moreover, the patterns of alternans can be either stationary, with fixed nodes, or travelling, with moving nodes and hence quasiperiodic oscillations of action potential duration, depending on the relative strength of the destabilizing effect of CV-restitution and the stabilizing effect of diffusive coupling. For the ring geometry, we recover the results of Courtemanche, Glass and Keener [M. Courtemanche, L. Glass, and J. P. Keener, *Phys. Rev. Lett.* **70**, 2182 (1993)] with two important modifications due to cell-to-cell diffusive coupling. Firstly, this coupling breaks the degeneracy of an infinite-dimensional Hopf bifurcation such that the most unstable mode of alternans corresponds to the shortest quantized wavelength of the ring. Secondly, the Hopf frequency, which determines the velocity of the node along the ring, depends both on the steepness of CV-restitution and the strength of this coupling, with the net result that quasiperiodic behavior can arise with a constant conduction velocity. In both the paced geometries and the ring, the onset of alternans is different in tissue than for a paced isolated cell. The implications of these results for alternans dynamics during two-dimensional reentry are briefly discussed.

PACS numbers: PACS numbers: 87.19.Hh, 05.45.-a, 05.45.Gg, 89.75.-k

## I. INTRODUCTION

It is well established that T wave alternans, defined as a periodic beat to beat change in the amplitude or shape of the ECG T wave [1], can be a precursor to life-threatening ventricular arrhythmias and sudden cardiac death [2]. T wave alternans have been related to alternations of repolarization at the single cell level [3], thereby establishing a causal link between electrical alternans and the initiation of ventricular fibrillation. Repolarization alternans are characterized by a beat to beat oscillation of the action potential duration ( $APD$ ) at sufficiently short pacing interval [4]. Experiments in both two-dimensional [3] and linear strands [5] of cardiac tissue, as well as ionic model simulations [5, 6, 7], have shown that the resulting sequence of long and short action potential durations can be either in phase along the tissue (concordant alternans), or can split into extended regions oscillating out of phase (discordant alternans). The latter case is of special importance since it can lead to conduction blocks [5] and the initiation of ventricular fibrillation [3]. Furthermore, alternans can provide a mechanism of wave breaks that sustain ventricular fibrillation [8]. The dual role of discordant alternans in the initiation and, potentially, the maintenance of fibrillation provides the motivation to develop a fundamental understanding of this phenomenon.

Experimental [9] and theoretical studies [10, 11] have shown that spatially modulated patterns of alternans associated with quasiperiodic oscillations of  $APD$  can arise naturally in a ring of tissue. The terminology of spatially “discordant alternans”, however, originates from the observation of such patterns in periodically paced tissue [3]. Their appearance in this context was first attributed to preexisting spatial heterogeneities in the electrophysiological properties of the tissue [3, 12]. Although heterogeneities may certainly be present [13], and can affect the formation of discordant alternans [6], numerical simulations of ionic models in homogeneous tissue [5, 6, 7, 14] have shown that they are not necessary for their formation. Dynamical properties alone are able to produce the spatially heterogeneous distributions of  $APD$  observed in the experiments.

Pioneering studies by Nolasco and Dahlen [15] and Guevara *et al.* [16] have demonstrated that the restitution relationship

$$APD^{n+1} = f(DI^n), \quad (1)$$

can account for alternans in a paced cell. Restitution relates the duration of the action potential generated by the  $n^{th} + 1$  stimulus,  $APD^{n+1}$ , with the diastolic time interval  $DI^n$ ,

during which the tissue recovers its resting properties after the end of the previous ( $n^{th}$ ) action potential. The restitution relationship only describes approximately the actual beat to beat dynamics because of memory effects that have been modeled phenomenologically through higher dimensional maps [17, 18, 19]. Moreover, recent theoretical studies have highlighted the role of intracellular calcium dynamics in the genesis of alternans [20, 21]. In the present paper, we will concentrate in models where the simple relationship given by Eq. (1) holds, but the general effect of memory will also be analyzed in the context of a two-dimensional map of the beat to beat dynamics.

If the time interval between two consecutive stimuli is fixed,  $\tau = APD^n + DI^n = const.$  for all  $n$ , then Eq. (1) yields the map  $APD^n = f(\tau - APD^{n-1})$  that has a period doubling instability if the slope  $f'$  of the restitution curve evaluated at its fixed point exceeds unity. This generically occurs as the pacing period is decreased, so there is a critical value of the pacing rate above which alternans develop. In extended tissue, the velocity of the activation wavefront also depends on  $DI$ , so the oscillations of  $APD$  induce oscillations in the local period of stimulation. This, in turn, acts as a control mechanism that tends to create nodes in the spatial distribution of  $APD$  oscillations, thus resulting in discordant alternans.

In a previous paper [22], we sketched the derivation of an amplitude equation that provides a unified framework to understand the initiation, evolution, and, eventually, control of cardiac alternans [23, 24]. For one-dimensional paced tissue, the equation takes the form

$$\tau \partial_t a = \sigma a - ga^3 - \frac{1}{\Lambda} \int_0^x a(x') dx' - w \partial_x a + \xi^2 \partial_x^2 a, \quad (2)$$

where  $a \simeq (APD^{n+1} - APD^n)/2$  measures the amplitude of period doubling oscillations in  $APD$ , so that nodes separating out-of-phase alternans region correspond to  $a = 0$ ,  $\tau$  is the pacing period,  $\sigma$  and  $g$  are coefficients that can be obtained from the map (1),  $\Lambda$  is related to dispersion in conduction velocity, and  $w$  and  $\xi$  are lengthscales that depend on the specific system considered. It should be noted that time can be treated as a continuous variable in this framework because, even though the APD oscillates from beat to beat, the amplitude  $a$  of this oscillation defined above varies over many beats close to the period doubling bifurcation. It is this slow spatiotemporal evolution that is described by Eq. 2.

In this paper, we provide a detailed derivation of the amplitude equation above and extend it to two-dimensional paced tissue. In addition, we extend this approach to treat the important case of one-dimensional reentry in a ring of tissue. For clarity of presentation, we

will first derive the amplitude equation for the ring geometry, and then show how to modify the boundary conditions on this equation to treat paced tissue in one and two dimensions. We also investigate memory effects that only modify the coefficients of the amplitude equation, but not its form. This modification, however, has important consequences for relating the genesis of discordant alternans to the underlying cell physiology.

The derivation of the amplitude equation follows the general amplitude equation framework that has been widely used to study the evolution of weakly nonlinear patterns in non-equilibrium systems [25]. In the present context of alternans, however, this derivation is made extremely difficult by the stiff nature of ionic models and the fact that the underlying stationary state (with no alternans) corresponds to a train of pulses. To surmount these difficulties, the derivation of the amplitude equation proceeds in two steps. First, spatially coupled maps, which describe the beat-to-beat dynamics of APD oscillations, including the crucial effect of cell-to-cell coupling, are derived from the underlying ionic models. Second, a weakly nonlinear and multiscale analysis is used to derive amplitude equations from these spatially coupled maps. The weakly nonlinear nature of the expansion is valid close to the onset of the period doubling bifurcation. The multiscale nature of the expansion, which allows to only retain the two lowest order spatial derivative terms in Eq. 2, is itself justified by the fact that the wavelength of spatial modulation of alternans is large compared to the scale  $\sim \xi$  over which the repolarization time course of a cell is influenced by neighboring cells through diffusive coupling.

The paper is organized as follows. In the next section, we introduce two ionic models and compute their action potential duration and conduction velocity restitution curves. These curves are used to relate quantitatively the ionic models and the amplitude equations. The models considered are the Noble model for Purkinje fibers [26] and a simple two-variable model ionic model that captures basic dynamical properties of the cardiac action potential. This model has the advantage that it is simple enough to calculate analytically the restitution curves as well as all the coefficients of the amplitude equation (2) analytically.

Section III is devoted to the derivation of the amplitude equation in the ring geometry. This equation is used to study the stability of pulses. The results are compared to previous analyses based on coupled maps [10, 11]. Courtemanche et al. [10] have shown that the wavelength of spatial modulation of alternans is quantized in a ring geometry. In the same language that has been used recently to describe discordant alternans in paced tissue, this

quantization condition corresponds, in the ring, to the existence of different modes of discordant alternans with an odd number of moving nodes separating out-of-phase regions of period doubling oscillations. The amplitude equation sheds light on the effect of cell-to-cell electrical coupling on the stability of these quantized modes of alternans. In particular, we find that this coupling lifts the degeneracy of an infinite-dimensional Hopf bifurcation so that the mode with one node is the most unstable, in qualitative agreement with the prediction of coupled maps that include a phenomenological description of cell-to-cell coupling [11]. Furthermore, we show that coupling can lead to quasiperiodicity even in the absence of conduction velocity (CV)-restitution, also known as dispersion in the excitable media literature. The effect of diffusive coupling on one-dimensional alternans dynamics in tissue has also been investigated in the context of a stability analysis of FitzHugh-Nagumo type models [27]. This analysis captures the fact that the onset of alternans in tissue can differ from a single cell. However, it does not provide a general framework to make predictions relevant for more realistic ionic models of cardiac excitation or experiments.

We extend our theory to the paced case in section IV. The main result is that discordant alternans result from a pattern-forming linear instability that produces either standing, with fixed nodes, or traveling waves, with moving nodes that separate out-of-phase alternans regions. Whereas in the ring the wavelength of discordant alternans is determined by the ring perimeter, the wavelength in the paced case is *independent* of tissue size. In the latter, spatial patterns form due to the competing effect of CV-restitution, contained in the nonlocal term in Eq. (2), which tends to create steep spatial gradients of repolarization, and diffusive cell-to-cell coupling contained in the spatial gradient terms, which tends to smooth these gradients. As a result of this competition, the wavelength  $\lambda$  of discordant alternans depends on the three fundamental length scales  $w$ ,  $\xi$ , and  $\Lambda$  in Eq. (2), with different scalings  $\lambda \sim (w\Lambda)^{1/2}$  and  $\lambda \sim (\xi^2\Lambda)^{1/3}$  for standing and travelling waves, respectively. In section IV, we also extend the model to two-dimensional paced tissue. This extension is straightforward under the assumption that the propagation of the front is weakly perturbed by the oscillations in *APD*. Finally, we discuss briefly nonlinear effects and conduction blocks.

Section V is devoted to memory. Although the ionic models we consider are well described by Eq. (1), in some cases a higher dimensional map is needed in order to reproduce the experimentally observed dynamics [18, 19, 28] or the effect of intracellular calcium cycling [20, 21]. In this case the onset of the period doubling is not linked to the slope of the

restitution curve in a simple way. In this section, we want to emphasize that our theory only relies on the system being close to the period doubling instability, and is perfectly valid in the presence of memory. Although we do not present an exhaustive study of this case, we sketch the derivation of the amplitude equations for a general memory model considered in the literature. One interesting result of this section is that the coefficient of the non-local term in Eq. (2) depends both on the slope of the CV-restitution curve and the beat-to-beat dynamics. This opens the possibility to prevent the formation of discordant alternans by modifying the dynamics at a single-cell level to make this coefficient negative, as would be the case for a negatively sloped “supranormal” CV-restitution curve when the single cell dynamics is governed simply by APD-restitution.

Finally, in sections VI and VII we present the discussion and conclusions.

## II. IONIC MODELS AND RESTITUTION CURVES

Our formulation is based on the action potential duration and conduction velocity restitution properties. To obtain the restitution curves, we simulate the ionic models in a one-dimensional strand of paced tissue. We consider the standard cable equation

$$\partial_t V = D \partial_x^2 V - (I_{\text{ion}} + I_{\text{ext}}) / C_m, \quad (3)$$

with the membrane current  $I_{\text{ion}}$ , time in units of millisecond (ms),  $D = 2.5 \times 10^{-4} \text{ cm}^2/\text{ms}$ ,  $C_m = 12 \mu\text{F}/\text{cm}^2$ . The external current  $I_{\text{ext}}$  models a sequence of stimuli applied at  $x = 0$  at a constant pacing interval  $\tau$ . We impose zero gradient boundary conditions on  $V$  at the two ends of the cable.

In the rest of the paper, we will use two models for the ionic currents: the original 1962 Noble model for Purkinje fibers [26], and a simplified two-variable model [22] defined by the total membrane current

$$\frac{I_{\text{ion}}}{C_m} = \frac{1}{\tau_0} (S + (1 - S)V/V_c) - \frac{1}{\tau_a} h S. \quad (4)$$

This current is the sum of a slow, time-independent, outward current (similar to the potassium current in more realistic ionic models), which repolarizes the cell on a slow time scale  $\tau_0$ , and a fast inward current that is a simplified version of the sodium current. The latter depolarizes the cell in the fast time  $\tau_a \ll \tau_0$ . The inactivation of the fast inward current is

regulated by the gate variable  $h$ , which evolves according to

$$\frac{dh}{dt} = \frac{(1 - S - h)}{(\tau_-(1 - S) + S\tau_+)}, \quad (5)$$

where  $\tau_+$  and  $\tau_-$  control the time scales of inactivation and recovery from inactivation of this current. In this model the transmembrane voltage  $V$  is dimensionless,  $S \equiv (1 + \tanh((V - V_c)/\epsilon))/2$  is a sigmoidal function, and we choose  $V_c = 0.1$ ,  $\tau_0 = 150$  ms,  $\tau_a = 6$  ms,  $\tau_- = 60$  ms,  $\tau_+ = 12$  ms, and  $\epsilon = 0.005$ . Note that  $\tau_-$  is larger than  $\tau_+$  owing to the fact that the product of the  $h$  and  $j$  gates in standard formulations of the sodium current is represented, in the present model, by a single gate  $h$ . Thus choosing  $\tau_-$  larger than  $\tau_+$  produces the same effect of a  $j$  gate that controls a slower recovery from inactivation in comparison to inactivation controlled by the  $h$  gate. As shown in Fig. 1, a typical action potential obtained with this model adopts a triangular form.

We have simulated Eq. (3) using the forward Euler method, with a three-point finite difference representation of the one-dimensional Laplacian. We take a mesh size  $dx=0.01$  cm, and a time step  $dt=0.02$  ms in the case of the two-variable model, and  $dx=0.01$  cm,  $dt=0.05$  ms, for the Noble model. The thresholds of the transmembrane voltage to define the *APD* are  $V = V_c = 0.1$  and  $V = -40$  mV, respectively. The restitution and dispersion curves are computed by pacing Eq. (3) in a short cable and by using two subsequent stimuli spaced by different intervals to vary  $DI$  (see Fig. 2).

In the limit in which the sigmoidal function  $S \equiv (1 + \tanh((V - V_c)/\epsilon))/2$  becomes a step function ( $\epsilon \rightarrow 0$ ), it is a straightforward exercise to calculate both the *APD*- and *CV*-restitution curves of the two-variable model analytically. Then, the single cell *APD*-restitution curve is (see Appendix A)

$$APD = \frac{\tau_+ \tau_0}{\tau_a} (1 - \exp(-DI/\tau_-)) - V_c \tau_0, \quad (6)$$

so the onset of alternans in a single cell is given by

$$\frac{dAPD}{dDI} = \frac{\tau_0 \tau_+}{\tau_a \tau_-} \exp(-DI/\tau_-) = 1, \quad (7)$$

or  $DI_c = \tau_- \log[(\tau_0 \tau_+)/(\tau_a \tau_-)]$  (resulting in  $DI_c = 96.6$  ms, and  $APD_c = 225$  ms, for the values we are considering).

The *CV*-restitution curve can be calculated considering a traveling pulse  $V(x, t) = V(x - ct)$ , and matching the expressions obtained for  $V > V_c$  and  $V < V_c$ , in the wavefront and

the waveback. This results in an implicit equation for  $c$ . When  $\tau_0$  is large, we can obtain an approximate expression of the conduction velocity by neglecting the effect of the outward current during depolarization, which is given by

$$c \simeq \sqrt{\frac{D}{V_c \tau_a} \left(1 - e^{-DI/\tau_-} - \frac{\tau_a V_c}{\tau_+}\right)} = c_\infty \sqrt{\frac{APD}{APD_\infty}}, \quad (8)$$

where we have defined  $APD_\infty = \tau_0(\tau_+/\tau_a - V_c)$ , and  $c_\infty = \sqrt{D[1/(V_c \tau_a) - 1/\tau_+]}$ , as the  $APD$  and conduction velocity of a front propagating along a tissue formerly in its rest state.

### III. RING GEOMETRY

The stability of pulses circulating in a ring of tissue was considered previously [10] using generic restitution properties of the system as given by Eq. (1). This stability analysis was based on the idea to unravel the ring into an infinite line (then  $x \in \mathcal{R}$ , instead of  $x \in \mathcal{R} \bmod L$ ), so space grows continuously with time. In this manner, the values of a given variable at a previous passage of the pulse through a given point  $x$  in the ring, and therefore, at a previous beat, can be identified with the value of that variable at the point  $x - L$  (i.e.  $APD^n(x) \equiv APD(x + nL)$ ). This allows to drop the dependence of the different variables on the beat number  $n$ , and reformulate the maps as delay differential equations. Using this approach it was found that, when the slope of the restitution curve is greater than one, the pulses become unstable towards modes of propagation where the values of the  $APD$  and conduction velocity vary in space around a mean value. Because of the periodic boundary conditions, these oscillations present an odd number of nodes. In the presence of dispersion  $c'[DI] \equiv d c / d DI \neq 0$ , the nodes travel, giving rise to quasiperiodic motion at a given point. In the analysis of [10] all the modes were found to bifurcate at the same time, in an infinitely degenerate Hopf bifurcation. This degeneracy was shown to be broken [11] by the effect of diffusive coupling, which effectively modifies the restitution relation (1) and makes the mode with lowest wavenumber (with a single node) bifurcate first. The effect of diffusive coupling was considered phenomenologically in [11], assuming a coupling of the  $APD$  in neighboring cells given by a gaussian kernel. This, however, misses an important point, the fact that the coupling is asymmetrical, due to the finite speed of propagation of the activation wavefront. In effect, the way a given cell is influenced by its left and right neighbors is different because these cells are activated at different times by the propagating

wavefront. Here we will show that, besides breaking the degeneracy of the instability, this asymmetry can also produce quasiperiodic motion, even in the absence of dispersion.

To study the stability of the pulses we will use an approach slightly different from that in [10]. We will convert the ring into a linear strand, cutting it at an arbitrary point, and index with  $n$  the number of times the pulse has traveled around the ring. Then, our fields will depend both on the beat number  $n$ , and on the space variable restricted to  $x \in [0, L]$ . This will allow us to consider both the ring and the paced case within a unified framework.

From the restitution curves a simplified description of the system in terms of coupled maps can be achieved, which will take the form:

$$T^n(x) = \int_{x-L}^x \frac{dx'}{c[DI^n(x')]} , \quad (9)$$

$$APD^{n+1}(x) = \int_{-\infty}^{\infty} G(x' - x) f[DI^n(x')] dx'. \quad (10)$$

The first equation is just a kinematic equation, stating that the period of stimulation at a given point is given by the time it takes a pulse to complete a revolution. The second equation reflects the restitution properties of the system, where we have included an asymmetrical kernel  $G(x' - x)$  that appears because of the diffusive coupling between neighboring cells. In general, the derivation of the kernel  $G(x' - x)$  is very difficult and we only derive it explicitly in Appendix A for our two variable model. The calculation of the kernel involves the inversion of a nonlocal, implicit equation for the  $APD$ . Even though we cannot derive this kernel for an arbitrarily complex ionic model, this is not a serious limitation since only the length scales  $w$  and  $\xi$ , but not the general form of the amplitude equation, depend on a precise knowledge of this kernel. Moreover,  $w$  and  $\xi$  can be calculated numerically.

### A. Linear stability revisited

Let us thus start reviewing the linear stability analysis of Eqs. (9) and (10). Taking into account that  $T^n(x) = APD^n(x) + DI^n(x)$  one can write Eqs. (9), (10) as a single equation for  $DI^{n+1}(x)$ :

$$DI^{n+1}(x) = \int_{x-L}^x \frac{dx'}{c[DI^{n+1}(x')]} - \int_{-\infty}^{\infty} G(x' - x) f[DI^n(x')] dx'. \quad (11)$$

Then, a stationary solution satisfies  $DI^* = \tau - f(DI^*)$ , where  $\tau = L/c(DI^*)$  is the period of propagation of the pulse, and we choose the kernel  $G(x' - x)$  to be normalized, so

$$\int_{-\infty}^{\infty} G(y) dy = 1. \quad (12)$$

Perturbing around the stationary solution in the form  $DI^n(x) = DI^* + \alpha^n e^{ikx} \delta D$ , and linearizing, it is easy to show that the following characteristic equation must be satisfied

$$\alpha = \frac{i\alpha}{2\Lambda k} (1 - e^{-ikL}) - f' G(k), \quad (13)$$

where we have defined the Fourier transform of the kernel

$$G(k) = \int_{-\infty}^{\infty} G(y) e^{iky} dy, \quad (14)$$

and  $\Lambda = c^2/(2c')$  is a characteristic length scale associated with dispersion, that can be computed from the CV-restitution curves.

Furthermore, from the condition  $D^{n+1}(x - L) = D^n(x)$  we obtain  $e^{ikL} = \alpha$ , so Eq. (13) can be rewritten as

$$\alpha(1 - \frac{i}{2\Lambda k}) = -f' G(k) - \frac{i}{2\Lambda k}. \quad (15)$$

The onset of the instability is given by  $|\alpha| = 1$ , that results into

$$f'^2 |G(k)|^2 + \frac{f'}{\Lambda k} \mathcal{Im}[G(k)] = 1. \quad (16)$$

When the kernel is symmetric, it follows that  $\mathcal{Im}[G(k)] = 0$ , and then  $f' = 1/|G(k)|$ . Assuming that the system evolves in a long spatial scale, and the kernel decays fast enough, the exponential in Eq. (14) can be expanded  $e^{iky} \simeq 1 + iky - (ky)^2/2 + \dots$ . Then

$$G(k) \simeq 1 - iwk - \xi^2 k^2, \quad (17)$$

where we have defined the coefficients

$$w = - \int_{-\infty}^{\infty} G(y) y dy, \quad \xi^2 = \frac{1}{2} \int_{-\infty}^{\infty} G(y) y^2 dy. \quad (18)$$

In a general situation, the kernel  $G(y)$  is not known, and  $w$  and  $\xi^2$  can be considered as two phenomenological coefficients that must be obtained from the numerical simulations of the ionic models. For the particular case of an ionic model with a constant repolarization rate,

as the two-variable model introduced before, they can be calculated explicitly (Appendix A), giving

$$w = 2D/c, \quad (19)$$

$$\xi = (D \times APD_c)^{1/2}. \quad (20)$$

Eq. (20) has the simple physical interpretation that the transmembrane potential  $V$  diffuses a length  $\sim \xi$  in the time interval of one  $APD$ . Therefore, the repolarization of a given cell is influenced by other cells within a length  $\sim \xi$  of cable. The imaginary part of  $G(k)$  appears because of the asymmetry induced by the propagation of the pulse. This asymmetry vanishes in the limit  $c \rightarrow \infty$ , where all cells are activated simultaneously, consistent with Eq. (19).

In what follows, and with no significant loss of generality, we will take the limit of small dispersion ( $1/\Lambda \ll 1$ ), and assume the scalings  $w \sim \xi^2 \sim 1/\Lambda$ . Then, up to first order in the expansion, the threshold for the instability becomes

$$f' \simeq 1 + \xi^2 k^2. \quad (21)$$

Intercellular coupling shifts the onset of instability, which occurs for a value of the slope of restitution  $f' \neq 1$ . Also, the first mode to bifurcate is that with largest wavelength, as already noticed in [11].

When  $\alpha = -1$ , this is, when the instability corresponds to period doubling, then the condition  $e^{ikL} = \alpha$  implies  $k = (2n + 1)\pi/L$ , with  $n = 0, 1, 2, \dots$ , and the motion at a given point is periodic. Both dispersion and asymmetrical coupling result in an imaginary part for  $\alpha$ , that corresponds to quasiperiodic motion. Assuming that these corrections are small, it is easy to show that  $\alpha$  becomes

$$\alpha \simeq -1 + iwk - \frac{i}{\Lambda k}, \quad (22)$$

and the corresponding wavenumber is

$$k = (2n + 1)\frac{\pi}{L} + \frac{1}{\Lambda(2n + 1)\pi} - w(2n + 1)\frac{\pi}{L^2}. \quad (23)$$

Therefore, besides the correction due to dispersion already noticed in [10], there is another one due to asymmetrical coupling, that produces quasiperiodic motion. In fact they can balance each other, if

$$w = \frac{L^2}{\Lambda(2n + 1)^2\pi^2}, \quad (24)$$

in which case the motion becomes strictly periodic.

## B. Derivation of the amplitude equations

Starting from the maps (9) and (10), it is possible to derive equations for the oscillations in period and action potential duration. To that end, we will consider the second iteration of the map (10), and expand it for small values of the amplitude of oscillation. As the change in the value of the *APD* every two beats is small, the beat number can be treated as a continuous variable. Also, the dispersion relation for the conduction velocity  $c = c(DI)$  can be expanded for small oscillations of  $DI$ , obtaining from Eq. (9) the corresponding change in the local stimulation period, that depends nonlocally on the oscillations of *APD*. The only non-trivial point in the expansion is the effect of electrical coupling in Eq. (10). Assuming that the kernel decays fast enough, we will expand it to obtain a local relation between the change in *APD* and its gradients at a given point.

Close to the onset of oscillations we can write

$$APD^n(x) \approx APD_c + (-1)^n a(x, t), \quad (25)$$

$$T^n(x) \approx \tau_c - \delta\tau + (-1)^n b(x, t), \quad (26)$$

where  $APD_c$  and  $\tau_c$  are the *APD* and the period of stimulation evaluated at the bifurcation point of the single-cell map ( $f' = 1$ ), and  $\delta\tau \equiv \tau_c - \tau \ll \tau_c$ . Now the basic pacing period will be the traveling time of a pulse around the ring, which in the absence of oscillations is given by  $\tau = L/c$ . Since the beat to beat oscillations are taken into account with the terms  $(-1)^n$ , the amplitude of the deviations from the critical values,  $a(x, t)$  and  $b(x, t)$ , vary slowly from beat to beat. We can therefore assume that  $a$  and  $b$  depend on a continuous time, defined through  $n \equiv t/\tau$ .

Let us first discuss what are the boundary conditions satisfied by  $a(x, t)$  and  $b(x, t)$ . The transmembrane voltage obeys periodic boundary conditions  $V(L) = V(0)$ , but, by definition, after a revolution of the pulse along the ring, the system goes into the next beat. Therefore, the values of the period and *APD* at  $x = L$  (this is, right before the end of the revolution) must equal those at  $x = 0$ , at the next beat (i.e. at the beginning of the next revolution). Then

$$T^n(L) = T^{n+1}(0), \quad (27)$$

$$APD^n(L) = APD^{n+1}(0). \quad (28)$$

Using Eqs. (25), (26) it is easy to see that, in terms of the oscillations in  $APD$  and period, the former boundary conditions become

$$a(L) = -a(0), \quad (29)$$

$$b(L) = -b(0). \quad (30)$$

It is clear, just from the boundary conditions, that the pattern must have an odd number of nodes. In effect, assuming  $a(x) \sim e^{ikx}$ , one gets the quantization condition

$$k = (2n + 1) \frac{\pi}{L}, \quad n = 0, 1, 2, \dots, \quad (31)$$

that was already obtained in [10] in the limit of zero dispersion. The corrections to the wavelength come from a phase shift in the slow scale, associated with the quasiperiodic motion.

The equation for the oscillations in period is easy to obtain. First, we can write Eq. (9) in differential form

$$\frac{dT^n(x)}{dx} = \frac{1}{c[DI^n(x)]} - \frac{1}{c[DI^n(x - L)]} = \frac{1}{c[DI^n(x)]} - \frac{1}{c[DI^{n-1}(x)]}, \quad (32)$$

where we have taken into account that  $DI^n(x - L) = DI^{n-1}(x)$ . Then, substituting expansions (25) and (26) into the former expression, with  $DI^n(x) = T^n(x) - APD^n(x)$ , we obtain, at linear order

$$\frac{db}{dx} = \frac{1}{\Lambda}(a(x) - b(x)), \quad (33)$$

with  $\Lambda \equiv c^2/(2c')$ , and  $c$  and  $c' \equiv dc/dDI$  evaluated at the bifurcation point. To obtain an expression for  $b(x)$  we have to solve Eq. (33), subject to the boundary condition (30). In order to be able to get an analytical expression for the shift in wavelength, we will take the limit of small dispersion ( $L/\Lambda \ll 1$ ), that will also allow us to compare with the results in [10]. It must be noted, however, that in the two-variable model this limit is not satisfied ( $L_c/\Lambda > 1$ ), and the full equation (33) should be considered if we want to get a satisfactory agreement with the results of the cable equation (3). As we are mostly interested in obtaining a qualitative understanding of the origin and dynamics of alternans, we will focus in the following in the limit of small dispersion, that simplifies the equations and makes analytical treatments possible. Then, neglecting the term proportional to  $b(x)$  in the right hand side of Eq. (33), and taking into account the b.c. (30) we obtain

$$b(x) = \frac{1}{\Lambda} \int_0^x a(x') dx' - \frac{1}{2\Lambda} \int_0^L a(x') dx'. \quad (34)$$

Next, in order to derive an evolution equation for the amplitude  $a(x, t)$ , we notice that, after two consecutive beats, the  $APD$  becomes

$$APD^{n+2} = APD_c + (-1)^{n+2}a(x, t + 2\tau). \quad (35)$$

Assuming that  $a(x, t)$  varies slowly from iteration to iteration (which is the case close to the period doubling bifurcation), we can expand  $a(x, t + 2\tau) \simeq a(x, t) + 2\tau\partial a/\partial t$ , so

$$APD^{n+2} = APD^n + (-1)^n 2\tau \frac{\partial a}{\partial t}. \quad (36)$$

But, expanding Eq. (10)

$$APD^{n+1}(x) = \int_{-\infty}^{\infty} G(y)f[DI^n(y+x)] dy \simeq f[DI^n(x)] - wf'\partial_x DI^n(x) + \xi^2 f'\partial_x^2 DI^n(x) \quad (37)$$

we can also write  $APD^{n+2}$  as

$$\begin{aligned} APD^{n+2} = & f[T^{n+1} - f(T^n - APD^n) + wf'\partial_x DI^n - \xi^2 f'\partial_x^2 DI^n] \\ & - wf'\partial_x(T^{n+1} - APD^{n+1}) + \xi^2 f'\partial_x^2(T^{n+1} - APD^{n+1}), \end{aligned} \quad (38)$$

where we have used the definitions in Eq. (18) for  $w$  and  $\xi^2$ . Then, using Eqs. (25)-(26), expanding to first order in  $w$  and  $\xi^2$ , and taking into account that  $f' = 1$ , since we are expanding around the period doubling bifurcation, we have

$$\begin{aligned} APD^{n+2} = & f[T^{n+1} - f(T^n - APD^n)] + w\partial_x DI^n - \xi^2 \partial_x^2 DI^n \\ & - w\partial_x(T^{n+1} - f(T^n - A^n)) + \xi^2 \partial_x^2(T^{n+1} - f(T^n - A^n)) \\ = & f[T^{n+1} - f(T^n - APD^n)] + (-1)^n \left\{ -w(2\partial_x a - 3\partial_x b) + \xi^2(2\partial_x^2 a - 3\partial_x^2 b) \right\} \end{aligned} \quad (39)$$

In the following we will neglect the term  $\partial_x b$  with respect to  $\partial_x a$ , since it would give terms of the type  $w a(x)/\Lambda$ , which we assume are of higher order in the limit of small dispersion. Strictly, the amplitude equation we derive is consistent with the scaling  $w \sim \xi^2 \sim 1/\Lambda \sim \delta\tau \sim a^2 \sim b^{2/3}$ .

Equating now Eq. (36) and (39), and expanding the second iteration of the map, we obtain the final expression for the evolution of the oscillations of  $APD$ , in the limit considered,

$$\tau\partial_t a = \sigma a - w\partial_x a + \xi^2 \partial_x^2 a - ga^3 - b, \quad (40)$$

where  $\sigma \equiv f''(\tau - \tau_c)/2$ ,  $g \equiv f''^2/4 - f'''/6$ , and all the derivatives are evaluated at the bifurcation point. These coefficients can be calculated from the curves in Fig. 2. It should

be noted that we find the bifurcation in the Noble model to be slightly subcritical, so Eq. (40) must be expanded to fifth order in this case [29]. For simplicity of exposition in the following we will focus on the supercritical case. When dispersion is not small, one should keep higher order terms in Eq. (40) involving the oscillation in period  $b$ . In that case direct simulation of the original coupled maps (9), (10) is probably more appropriate, if the goal is to achieve good quantitative agreement.

Substituting the expression for  $b(x)$  into Eq. (40), we obtain the final amplitude equation in the ring geometry

$$\tau \partial_t a = \sigma a - g a^3 - w \partial_x a + \xi^2 \partial_x^2 a - \frac{1}{\Lambda} \int_0^x a(x') dx' + \frac{1}{2\Lambda} \int_0^L a(x') dx', \quad (41)$$

that must be solved with the boundary condition  $a(L) = -a(0)$ .

Now, we can consider again the linear stability problem, within our amplitude equation framework. To do that, we write  $a(x) \sim e^{ikx+\Omega t}$ , with  $k$  given by (31), and  $\Omega$  complex ( $\Omega = \Omega_r + i\Omega_i$ ). Separating into real and imaginary parts

$$\tau \Omega_r = \sigma - \xi^2 k^2 = \sigma - \frac{\xi^2}{L^2} (2n+1)^2 \pi^2, \quad (42)$$

$$\tau \Omega_i = \frac{1}{\Lambda k} - wk = \frac{L}{\Lambda} \frac{1}{(2n+1)\pi} - \frac{w}{L} (2n+1)\pi. \quad (43)$$

The onset of instability occurs when  $\Omega_r = 0$ , which results into  $\sigma = \xi^2 k^2$ , equivalent to condition (21). Again, we see that intercellular coupling lifts the degeneracy in the onset of the different modes, since the growth rate depends on the wavenumber of the mode. Clearly, the fastest growing mode is that with the largest wavelength, which corresponds to the mode with a single node. Intercellular coupling also affects the frequency of the quasiperiodic oscillations. For the parameters of the two-variable model, Eq. (43) gives  $\Omega_i = 1.38 \cdot 10^{-3} \text{ ms}^{-1}$ , which results in a velocity of the nodes (equal to the phase velocity)  $v = -\Omega_i/k = -2.27 \cdot 10^{-3} \text{ cm/ms}$ , while from the direct numerical simulations of the ionic model we obtain  $v = -\Omega_i/k = -1.81 \cdot 10^{-3} \text{ cm/ms}$ . The discrepancy is due to  $1/\Lambda$  corrections, since it is possible to obtain a modified expression for  $\Omega_i$  starting from the full equation (33), that gives an almost perfect agreement with the numerical results.

To compare Eqs. (42), (43) with the results from the linear stability of the maps in the previous section, we can factor out the rapid oscillations, so  $\alpha^n = (-1)^n \beta^n = (-\beta)^n$ , and  $\beta^n = e^{\Omega t} = e^{\tau \Omega n}$ , by the definition of the slow time  $t = n\tau$ . Then, at onset of the instability,

$\Omega = i\Omega_i$ , and

$$\alpha = -\beta = -e^{i\tau\Omega_i} \simeq -1 + i\omega k - \frac{i}{\Lambda k} \quad (44)$$

which is exactly the expression we had obtained before (cf. Eq. (22)).

Close to onset, the bifurcating solution is therefore in the form of traveling waves

$$a(x) = \frac{1}{2}(Be^{i(kx+\Omega_i t)} + c.c.), \quad k = \pi/L, \quad (45)$$

with an amplitude given by

$$|B| = \sqrt{\frac{4(\sigma - \pi^2 \xi^2/L^2)}{3g}}. \quad (46)$$

#### IV. PACED TISSUE

The main difference between the ring and the paced case comes from the role of the boundary conditions. While in the ring the periodic boundary conditions result in a quantization condition for the unstable modes, such a condition is absent in the paced case. Thus, the selected wavelength in this latter case must be related to some intrinsic length scale of the system. We show in Fig. 3 simulations of both the Noble and two-variable models, close to onset. Although physiologically unrealistic, we have done simulations in very large tissues to stress the striking spatial regularity of the oscillations in *APD*. This seems to suggest that these patterns appear through a pattern forming instability of the basic underlying state, similar to those encountered in other physico-chemical systems, such as Rayleigh-Bénard convection, Taylor-Couette flow, etc [25]. Results in more realistic tissue sizes (where alternans can be concordant in small tissues, or discordant, for larger lengths), present exactly the same length scale. The *APD* oscillations obtained with the Noble model resemble a standing wave (Fig. 3c), and those for the two-variable model a traveling one (Fig. 3d). Thus, at a given point in the tissue, the oscillations in *APD* are periodic in the first case, and quasiperiodic in the second. We will see how within the formalism of the amplitude equations these length scales appear naturally.

To derive the amplitude equations for the paced case, we must notice that the equations in the bulk remain the same (cf. Eq. (40)), and we only have to modify the boundary conditions. Again, the only problem here comes from the spatial coupling. In fact, in the derivation in the ring, we use translational symmetry to expand the kernel. In the paced case this symmetry is broken and one should, in principle, calculate the kernel for the finite

system. When the decay rate of the kernel is fast this does not seem to be necessary. The same equations, supplemented with non-flux boundary conditions for the oscillations of *APD*, give a remarkably good agreement with simulations of the ionic models, for all the lengths of tissue considered in this paper. It is interesting to notice that the *APD* itself does not satisfy these boundary conditions, as blips appear at the two ends of the cable, due to the non-flux boundary conditions for  $V$ . The difference between two consecutive beats, however, does indeed satisfy them very well, as can be checked from numerical simulations of the ionic models. For very small system sizes, however, we would expect this approach to fail, as finite size effects become important. We have not investigated this point. Neither have we tried to formally derive the boundary conditions from the finite size kernel.

The condition that the period must be equal to the pacing interval at  $x = 0$ ,  $T^n(0) = \tau$ , translates into  $b(0) = 0$ . Then, Eq. (33) can be solved for  $b(x)$  to give

$$b(x) = \frac{1}{\Lambda} \int_0^x e^{(x'-x)/\Lambda} a(x') dx'. \quad (47)$$

As in the previous section, we will assume that the *CV*-restitution curve is shallow at the bifurcation point, so  $\Lambda$  is much larger than the wavelength of the pattern ( $\Lambda \gg 2\pi/k$ ). If this is the case the exponential in (47) can be neglected and the former relation becomes

$$b(x) \simeq \frac{1}{\Lambda} \int_0^x a(x') dx'. \quad (48)$$

Introducing this into Eq. (40), we arrive at the final expression

$$\tau \partial_t a = \sigma a - g a^3 - \frac{1}{\Lambda} \int_0^x a dx' - w \partial_x a + \xi^2 \partial_x^2 a. \quad (49)$$

With the help of equation (49) the formation of the nodes is easy to explain. Let us first neglect the influence of the electrical coupling between cells on the *APD* (that later on will be shown to be crucial), and consider the equation

$$\tau \partial_t a = \sigma a - g a^3 - b. \quad (50)$$

Starting at  $x = 0$  with a constant amplitude of oscillation for the *APD*  $a$ , the oscillation in the period  $b$  will increase along the tissue (cf. Eq. (48)), effectively decreasing the value of  $a$ , until it crosses zero and goes into the branch with opposite phase (see Fig. 4). Thus, the system tends to create discordant alternans spontaneously, through *CV*-restitution. However, without the derivative terms the gradients become ever steeper, until

they form singularities. To see this, we can differentiate Eq. (50), to obtain the steady state equation for the slope of the oscillations in  $APD$   $\partial_x a = a/\Lambda(\sigma - 3ga^2)$ . When  $a^2 = \sigma/3g$  the slope becomes infinite, denoting the formation of a singularity, with the distance between singularities given by  $\lambda/2 = \Lambda f''(1 - \ln \sqrt{3})\delta\tau$ . The singular behavior originates from the use of the local  $APD$ -restitution relation (Eq. (1)) that allows two nearby cells to have different  $APDs$ , whereas this is prevented in the cable equation by the spatial diffusive coupling. Furthermore, the distance between singularities obtained from Eqs. (48), (50) does not correspond to the right length scale for this problem (compare Figs. 4 and 3). Once the derivative terms are included, the agreement between the ionic models and the amplitude equations becomes very good.

To check this point, we have derived the coefficients  $w$  and  $\xi^2$  from the restitution curves of the Noble model (in the two-variable model are given by Eqs. (19) and (20)). The coefficient  $w$  can be derived from the splitting of the dynamic restitution curves in alternating beats (see Fig. 5), if we know the value of the gradient  $\partial_x a$  (that we have measured from Fig. 3c). Assuming that the gradient evaluated at the critical value of the  $APD$  has the same magnitude but opposite sign at two consecutive beats, then:

$$w \simeq \frac{APD^{n+1} - APD^n}{\partial_x APD^n - \partial_x APD^{n+1}} = \frac{\Delta APD_1}{2\partial_x a}. \quad (51)$$

The value of  $APD_1$  is measured at a point where  $APD = APD_c$ , so the slope of  $APD$  is constant, and the contribution from the second derivative is negligible.

The coefficient  $\xi^2$ , by the other hand, is proportional to the shift of the dynamic restitution curve, with respect to that obtained using a S1-S2 protocol (see Fig. 5), where gradients are absent. In this case

$$\xi^2 \simeq -\frac{\Delta APD_2}{\partial_x^2 a}, \quad (52)$$

where the second derivative is calculated at the maximum value of the  $APD$  in Fig. 3c, so the contribution from the first derivative is negligible. In Table I we show the values of the coefficients calculated in this manner. The comparison between simulations of the amplitude equation (49) using these coefficients and the Noble equations is very good, as shown in Fig. 6.

TABLE I: Values of various lengths in cm with  $\lambda_{theor}$  (Eq. (55) or Eq. (58)) and  $\lambda_{sim}$  (from simulations of Eq. (3)). The values of  $\Lambda$  are obtained from the CV-restitution curves computed numerically.

Model	$\Lambda$	w	$\xi$	$\lambda_{theor}/4$	$\lambda_{sim}/4$	$L_{min}$
Noble	49.1	0.045	0.18	2.33	2.6	2.75
Two-variable	3.55	0.031	0.235	1.33	1.1	1.15

### A. Linear stability analysis

Although nonlinear effects are important to saturate the oscillating state and can somehow modify the distance between nodes, most of the characteristics of discordant alternans (its wavelength and, in the case of traveling nodes, its phase velocity) are already selected at the linear level.

The genesis of discordant alternans can be understood by computing the linear stability spectrum of the spatially homogeneous state ( $a = 0$ ). We have calculated this spectrum both numerically for different  $L$ , and analytically for the large  $L$  limit. The main result is that the wave pattern can emerge from the amplification of *either* a unique finite wavelength mode, which yields a stationary pattern, *or* from a discrete set of complex modes that approach a continuum in the limit  $L \rightarrow \infty$ , and yields a traveling pattern (see Fig. 3). There is indeed experimental evidence for both stationary [3] and traveling [5] waves.

To obtain the linear spectrum for a given value of  $L$ , we have linearized and discretized in space Eq. (49), using a finite difference representation of the derivatives and the trapezoidal rule for the integral. Looking for exponentially growing or decaying solutions  $a_i(t) \sim a_i e^{\Omega t/\tau}$ , we obtain a set of  $N$  coupled linear algebraic equations

$$\Omega a_i = \sigma a_i - \frac{w}{2dx}(a_{i+1} - a_{i-1}) + \frac{\xi^2}{dx^2}(a_{i+1} + a_{i-1} - 2a_i) - \frac{dx}{\Lambda} \sum_{j=0}^{i-1} \frac{1}{2}(a_j + a_{j+1}), \quad i = 1 \dots N, \quad (53)$$

where  $L = Ndx$ , and we typically use  $dx=0.1\text{cm}$ . The non-flux boundary conditions now become  $a_0 = a_2$ , and  $a_{N+1} = a_{N-1}$ . The resulting eigenvalue problem is then solved for the complex growth rate  $\Omega = \Omega_r + i\Omega_i$ , and the corresponding eigenmodes.

For the parameters of the Noble model, and small values of  $L$ , the most unstable mode does not present any node, and there is a band of stationary modes, with growth rate of the form  $\Omega_r \simeq \sigma - \xi^2 k^2$ , where we calculate the wavenumber from the number of nodes  $n$ , as

$k \simeq \pi(2n-1)/(2L)$ . As the length of the tissue is increased, a point is reached at which the most unstable mode develops a node. This mode, however, does not belong to the discrete set, being an isolated eigenvalue (see Fig. 7a). Further increasing  $L$ , the longwavelength modes become oscillatory, and, in the limit  $L \rightarrow \infty$ , the spectrum consists of a real isolated eigenvalue plus a continuum of complex modes.

For the two-variable model the sequence is similar, with the important difference that, in this case, the isolated eigenvalue never appears, and only the continuum branch remains. Increasing  $L$ , the maximum of the branch shifts from a mode without a node to a complex mode with one node, the whole branch becoming complex as  $L \rightarrow \infty$ . In this limit the instability resembles a typical pattern-forming instability, with the maximum of the curve going above zero for some critical value of the pacing rate (Fig. 7b).

In the large  $L$  limit it is possible to obtain analytical expressions for the wavenumber and onset of the waves, by differentiating Eq. (49) with respect to  $x$  and letting  $a(x, t) \sim e^{ikx+\Omega t/\tau}$ , with both  $\Omega \equiv \Omega_r + i\Omega_i$  and  $k \equiv k_r + ik_i$  complex, which yields at once the eigenvalue equation

$$\Omega = \sigma - \xi^2 k^2 - i \left[ wk - \frac{1}{\Lambda k} \right]. \quad (54)$$

When dispersion is weak, a unique real mode with  $k_i = 0$  grows faster than the other complex modes and yields a stationary pattern. Its wavelength  $\lambda = 2\pi/k_r$ , is determined by the condition  $\Omega_i = 0$ , which yields

$$\lambda = 2\pi(w\Lambda)^{1/2}, \quad (55)$$

in good agreement with the wavelength observed in simulations of the cable-Noble equation (Table I). Note that  $\cos k_r x$  is an exact eigenvector of Eq. (49) linearized around  $a = 0$  that satisfies  $\partial_x a = 0$  at the two cable ends when  $L$  is an integer multiple of  $\lambda/2$ . The threshold of instability occurs when  $\Omega_r = 0$ , or for a period  $\tau_{th}$  defined by  $\sigma_{th} \equiv f''(\tau_{th} - \tau_c)/2 = \xi^2/(w\Lambda)$ .

If  $w \rightarrow 0$ , or dispersion is stronger, so it cannot be balanced by the drift term, then complex modes that grow exponentially at large  $x$  are the most unstable. It is simple to deduce from Eq. (54) that each  $k$ -mode travels towards the pacing end of the cable, but a wave-packet constructed from a linear superposition of these modes has a group velocity that makes the packet move away from the pacing end. This is the signature of a convective instability [25] where perturbations are transported as they grow, similarly to, for instance, Taylor-Couette vortices developing in an axial flow [30]. In such a situation, patterns are

only transient unless the group velocity vanishes [31], or  $\partial\Omega_i/\partial k_r = 0$ , and hence they grow at a fixed point in space (see Fig. 8). Fig. 9 illustrates sustained and transient wave patterns above (left) and below (right) the onset of absolute stability, respectively. Moreover, the fastest growing wavelength that dominates at large time must correspond to a maximum of  $\Omega_r$ , which yields the additional condition  $\partial\Omega_r/\partial k_r = 0$ . These two conditions are equivalent to requiring that

$$\frac{d\Omega}{dk} = 0 = -2\xi^2 k - iw - \frac{i}{\Lambda k^2}. \quad (56)$$

From this equation we can calculate the (complex) wavenumber for the onset of instability. In the limit  $w \rightarrow 0$ , it becomes simply

$$k = \pm \frac{\sqrt{3}}{2(2\xi^2\Lambda)^{1/3}} - \frac{i}{2(2\xi^2\Lambda)^{1/3}}, \quad (57)$$

so it corresponds to modes growing exponentially in space. This is already evident in Fig. 3c, where the amplitude away from the pacing point has saturated.

Substituting this expression into Eq. (54), we deduce that the threshold of absolute instability occurs when  $\sigma_{th} = (3/2)(\xi/2\Lambda)^{2/3}$ , with a pattern of wavelength

$$\lambda = \frac{4\pi}{\sqrt{3}}(2\xi^2\Lambda)^{1/3}, \quad (58)$$

which travels with phase velocity  $v_{ph} = -\Omega_i/k_r$ , where  $\Omega_i = (3\sqrt{3}/2)(\xi/2\Lambda)^{2/3}$ . This wavelength agrees well with that observed in simulations of the two-variable model (see Table I). It can also be deduced that traveling waves are favored over a stationary pattern when  $\Lambda = c^2/(2c') \ll \xi^4/w^3$ , and hence for large enough dispersion ( $c'$ ), and vice versa in the opposite limit.

Thus, our results demonstrate that the formation of discordant alternans is crucially affected by the effect of electrical coupling (diffusion) on repolarization, in addition to restitution and dispersion. Dispersion is responsible for the formation of nodes and spatial gradients of *APD* that steepen with time. Diffusion, in turn, tends to spread the *APD* spatially, and also induces a drift of the pattern away from the pacing site that is induced by the more subtle gradient term  $(-w\partial_x a)$  in the amplitude equation. When dispersion is sufficiently weak, it may be balanced by drift and produce a stationary pattern. In the opposite limit, the tendency for dispersion to form steep gradients of *APD* is balanced by the spreading effect of diffusion. Nodes then travel, cyclically disappearing (appearing) at the pacing (opposite) end of the cable.

It is interesting to notice that the length scale for the standing waves in the paced case is the same as that for the strictly periodic motion in the ring (see Eq. (24)). In the former case, however, the non-flux boundary conditions pinned the node (imposed  $\Omega_i = 0$ ), and that was the only possible wavelength for a bounded state. The only possibility of having a different wavelength, and a traveling node, was to pick up an exponential part ( $k$  complex), which is precluded in the ring by the boundary conditions. There, the wavelength is selected by the boundary conditions, and depends on the length of the system. This, in turn, selects the velocity of the node through Eq. (43), that in general will be different from zero. Comparing the critical length scales in both cases, we see that for the mode with largest wavelength in the ring ( $n = 0$ ), this results in a critical tissue length of  $L_c = \lambda/2 = 5.78\text{cm}$ , for Noble, and  $L_c = \lambda/2 = 5.17\text{cm}$  for the two-variable model. Thus, the length scale in the ring is comparable with that in the paced case for the Noble model, while for the two-variable model it is significantly larger (see Table I).

## B. Stability diagrams

To compare with previous numerical and experimental results we have calculated the different solutions of the Noble and two-variable models as a function of cable length  $L$  and pacing period  $\tau$ . As can be seen in Fig. 10 these results are in good agreement over a wide range of  $L$  and  $\tau$  with those obtained simulating the amplitude equations. In particular, discordant alternans appear as soon as the cable is long enough to accommodate a fourth of a wavelength, as given by expressions (55) and (58) (see Table I). Several comments are in order regarding our results.

(i) The transition from concordant to discordant alternans occurs as the length of the tissue is increased, but the transition line remains nearly constant with increasing pacing rate. This seems to contradict the results obtained in [3], where a transition from concordant to discordant alternans was reported as the pacing rate was increased. In typical models, the slope of  $CV$ -restitution is small for large values of  $DI$ , but increases very rapidly for small values of  $DI$  (see, for instance, the  $CV$ -restitution curve of the Noble model in Fig. 2b). Thus, as the pacing rate is increased and the amplitude of oscillation grows, eventually the system begins to pick up the steep part of the  $CV$ -restitution curve, at which point a sudden transition to discordant alternans occurs. In the Noble model, this never happens,

since there is a reverse period-doubling bifurcation at larger pacing rates that does not allow the oscillations to grow enough, but we have checked this point with simulations of the Beeler-Reuter equations (not shown here). Within our amplitude equations this effect can not be captured since we are expanding around the critical point, where the slope of the  $CV$ -restitution is fixed. However, it can be observed with the coupled map equations (1), (9) (that must be supplemented with some regularization to prevent singularities), where the whole restitution curves are used.

(ii) Discordant alternans appear directly from the rest state. This was already observed in simulations of the Beeler-Reuter model [7], for lengths of tissue  $L \gtrsim 5$  cm. As can be seen in Fig. 5 of that paper, the number of nodes increases with the size of the tissue. This is also the case in our simulations of the Noble model (Fig. 3), where, close to onset, the oscillations of  $APD$  adopt a sinusoidal form, with a well defined wavelength. A similar result was observed in [6], where the Luo-Rudy model was modified to obtain several  $APD$  and  $CV$ -restitution curves. In agreement with our results, when the slope of  $CV$ -restitution was large at onset, a direct transition to discordant alternans was observed, while, in the case of a shallower curve, the primary transition was to concordant alternans, discordant alternans only appearing when the oscillations in  $APD$  grew enough to explore the steep part of the  $CV$ -restitution curve.

(iii) The onset of alternans in an extended tissue is delayed with respect to that of the single cell (as given by Eq. (1)). This restabilizing effect has to do with  $CV$ -restitution, that induces oscillations in the period of stimulation that effectively act as a control mechanism. In Eq. (49) this effect is produced by the integral term. As is readily seen in Fig. 10 from the diagrams of the Noble and two-variable models, the larger the slope of  $CV$ -restitution is at the critical point  $f' = 1$  (the smaller  $\Lambda$  is), the larger the value of the restabilization.

(iv) The nodes separating regions oscillating out of phase may be stationary (Noble model), or traveling (two-variable model). Since this distinction occurs already at onset, and there is no transition from one case into the other as the pacing rate is increased, the selected type must depend on the specific ionic model considered. There is experimental evidence for both types of patterns [3, 5]. It should be noticed, however, that in real tissue other effects not considered here, such as gradients of restitution properties, could be important, and affect the motion of the node. In the experiments in [5] the tissue was paced from both ends, with identical results, which seems to suggest that gradients are not important in that

case. In other situations, however, the gradient terms could become important, and create a drift that opposes or reinforces the effect of dispersion.

### C. Nonlinear state: conduction blocks and front solutions

Nonlinearities are mainly responsible for saturating the amplitude of the linear modes, although both the wavelength and evolution of the pattern can generally vary with distance from onset. Furthermore, at high amplitudes conduction blocks can be produced, which are the main mechanism for the induction of reentry. Recently, systems of coupled maps such as given by Eqs. (1) and (9) have been used to study the appearance of conduction blocks [32, 33, 34]. They are often produced right after the first node in the *APD* oscillations [32], thus stressing the importance of discordant alternans for the induction of conduction blocks. Furthermore, it has been shown that the position of the wave block travels if the system presents traveling nodes [33].

Although strictly valid only close to onset, we will use our amplitude equations to get an idea on where conduction blocks can be formed. A conduction block occurs wherever the *APD* is large enough, so  $D = \tau - APD < D_{min}$ , being  $D_{min}$  the minimum diastolic interval necessary for propagation. Let us, to start, do not take into account diffusive effects. Then, using Eq. (50), which is the amplitude equation corresponding to the maps (1) and (9), it is easy to show that the maximum value of the *APD* occurs just after the discontinuity (see Fig. 4). From

$$\partial_x a = \frac{a}{\Lambda(\sigma - 3ga^2)} \quad (59)$$

we obtain that the discontinuity occurs when  $a^2 = 3\sigma/g$ . At that point  $b = \sigma a - 3ga^3 = -2\sigma^{3/2}/(3\sqrt{3g})$ , if we take the minus sign for  $a$ . As  $b$  is continuous through the discontinuity of *APD* (Fig. 4), the value of  $a$  after the discontinuity can be calculated from

$$ga^3 - \sigma a + b = 0, \quad (60)$$

which gives  $a = 2\sqrt{\sigma/3g}$ . Then, the conduction block occurs at a value of the period implicitly given by

$$D_{min} = \tau - A_c - 2\sqrt{\sigma/3g}, \quad \text{with } \sigma = \frac{1}{2}f''(\tau - \tau_c), \quad (61)$$

and at a point in space given by the position of the first singularity, or

$$x_0 = \frac{1}{2}\Lambda(1 - \ln \sqrt{3})f''(\tau - \tau_c). \quad (62)$$

One should be very careful when considering this latter result, since the inclusion of diffusive effects changes the position of the node, and can make it travel. The reason is that, without diffusion, arbitrarily steep gradients can develop, that prevent the node from moving. Once diffusive effects are included, this is no longer the case, and the node travels, unless its motion is balanced by the drift term. In fact, there is a close analogy between the amplitude equation (49) and the real Ginzburg-Landau equation that has been extensively studied in the context of phase transitions and front propagation [25]. The dynamics is richer here because the integral term originating from dispersion causes a non-local interaction of the fronts separating two out-of-phase oscillating regions with the pacing end of the cable. When dispersion is small, it is easy to show that the motion of the node is given by

$$\tau \frac{dx_0}{dt} = w - \frac{3}{\Lambda} \sqrt{\frac{\xi^2}{2\sigma}} x_0. \quad (63)$$

For arbitrary dispersion the expression for the motion becomes more complicated, but the effect is essentially the same. The gradient term corresponding to  $w$  makes the node move with constant velocity away from the pacing point, while the integral term provides a ramp that tilts the free energy and makes one phase preferred over the other. When dispersion is weak, there is a point at which the two effects balance and the node ends up at the equilibrium position:

$$x_0^{eq} = \frac{w\Lambda}{3} \sqrt{\frac{2\sigma}{\xi^2}}, \quad (64)$$

different from that given in Eq. (62). When the product  $w\Lambda$  is small, the equilibrium position may become closer to the pacing point than the width of the front, at which point it is absorbed, resulting in a traveling node.

#### D. Two-dimensional paced tissue

Let us now generalize our formalism to the case of a square piece of tissue paced at one corner. The equivalent of Eq. (40) is simply

$$\tau \partial_t a = \sigma a - g a^3 - b - w (\hat{\mathbf{n}} \cdot \nabla) a + \xi^2 \nabla^2 a, \quad (65)$$

where  $\hat{\mathbf{n}}$  is a unit vector normal to the direction of propagation of the wavefront, and we impose non-flux boundary conditions on the boundaries of the tissue.

Now the determination of the period at a given point would involve the integral along the path traveled by the wavefront. In particular, we obtain the condition for the oscillations in period:

$$(\hat{\mathbf{n}} \cdot \nabla)b = \frac{a}{\Lambda}. \quad (66)$$

In general this is a complicated problem, since we have to know the normal to the wavefront at any given point. A major simplification occurs if we assume that the oscillations in *APD* do not affect the form of the propagating wavefront, which is the same as to say that the azimuthal variations of *APD* are small compared with the radial ones. Then, as long as the thickness of the wavefront is small compared with the size of the tissue, it can be assumed that, except for narrow boundary layers at the borders of the tissue, the propagation of the wavefront is perfectly circular. In this case, Eq. (65) can be rewritten as:

$$\tau \partial_t a = \sigma a - g a^3 - \int_0^r a dr' - w \partial_r a + \xi^2 \nabla^2 a. \quad (67)$$

In the far field limit, these equations reduce to Eq. (49), with the node now becoming a circular line. We therefore expect to be a minimum tissue size for the node to form (Fig. 11a), as in the one-dimensional case. This was already observed in experiments [3] and numerical simulations of ionic models [7], where after a few beats, a nodal line was formed at the corner opposite the pacing point, and then moved towards it. Close to the pacing point, however, the motion of the node becomes nontrivial, because of curvature effects. Besides the term  $-w \partial_r a$  that tends to make the nodal line move in the radial direction away from the pacing point, there is a contribution to the drift in the direction normal to the interface coming from the laplacian, this being positive or negative depending on the curvature of the interface. As the nodal line is always perpendicular to the boundaries, its curvature depends on its position on the square. When the tissue is large enough so in the one-dimensional case the node would form in the region with positive curvature (close to the pacing point), this extra effect may be enough to make it travel (Fig. 11).

## V. MEMORY

Recently several experimental and theoretical works have stressed the fact that the slope of the restitution curve is not always a good indicator of the transition to alternans [18, 19, 28]. This is typically related with the existence of memory effects, that introduce extra variables in the map (1), with their own dynamics described by a set of coupled maps. Then, the onset of alternans is no longer given by the slope of the restitution curve being equal to one, but by the corresponding condition resulting from the linearization of the higher dimensional map. We want to emphasize that our theory does not rely on the restitution relation (1), but is also valid for any higher dimensional map close to a period doubling bifurcation. To illustrate this point, let us consider the model proposed in [18] (one could straightforwardly translate the following arguments to similar memory models [19, 35])

$$APD^{n+1} = f(DI^n, M^n) = c_1(1 - M^n)[1 - c_2 e^{DI^n/\tau_1}], \quad (68)$$

$$M^{n+1} = g(M^n, DI^n, APD^n) = [1 + (M^n - 1)e^{-APD^n/\tau_2}]e^{-DI^n/\tau_2}, \quad (69)$$

that includes a memory term  $M$  that describes the long term evolution of the tissue properties. We will not consider specific values in the maps above, but rather sketch how to derive amplitude equations similar to (40) for such coupled maps.

To include spatial effects, we will assume that diffusive coupling enters only in the map for the  $APD$ , which then becomes:

$$APD^{n+1}(x) = \int G(y)f[DI^n(x+y), M^n(x+y)]dy \simeq f[DI^n(x), M^n(x)] - w(f_{DI}\partial_x DI^n(x) + f_M\partial_x M^n(x)) + \xi^2(f_{DI}\partial_x^2 DI^n(x) + f_M\partial_x^2 M^n(x)) + \dots \quad (70)$$

### A. Linear stability of the coupled maps

We will consider the stability of steady state homogeneous solutions  $APD^* = f(\tau - APD^*, M^*)$ ,  $M^* = g(M^*, \tau - APD^*, APD^*)$ , at a given value of the pacing period  $T^n = \tau$ . Perturbing around these solutions

$$APD^n = APD^* + \alpha^n \delta A, \quad M^n = M^* + \alpha^n \delta M, \quad (71)$$

we obtain the following eigenvalue system:

$$\begin{pmatrix} -f_{DI} - \alpha & f_M \\ g_{APD} - g_{DI} & g_M - \alpha \end{pmatrix} \begin{pmatrix} \delta A \\ \delta M \end{pmatrix} = \begin{pmatrix} 0 \\ 0 \end{pmatrix} \quad (72)$$

and the corresponding characteristic equation:

$$(f_{DI} + \alpha)(g_M - \alpha) - f_M(g_{DI} - g_{APD}) = 0, \quad (73)$$

where the subindex indicates derivative with respect to that variable. In order to have a period doubling instability ( $\alpha = -1$ ), the following condition must then be satisfied

$$f_{DI} = 1 + \frac{f_M(g_{DI} - g_{APD})}{1 + g_M}. \quad (74)$$

The condition  $f_{DI} = 1$  is recovered in the cases  $f_M = 0$  or  $g_{APD} = g_{DI} = 0$ , where the system becomes decoupled (at linear level), and also when  $g_M \rightarrow \infty$ , in which case the variable  $M_n$  can be adiabatically eliminated. When none of these conditions is satisfied, the dynamics of the *APD* and memory function is interlinked, and one has to solve the corresponding eigenvalue problem to find the mode related with the instability. Setting  $\alpha = -1$  in (72), we obtain that the mode undergoing the period doubling bifurcation is given by:

$$v_r^u = \begin{pmatrix} 1 \\ -\frac{1-f_{DI}}{f_M} \end{pmatrix}. \quad (75)$$

As we are considering a two dimensional system, there will be a second eigenvalue, given by  $\alpha = g_M - f_{DI} + 1$ , with the corresponding eigenvector

$$v_r^s = \begin{pmatrix} \frac{1-f_{DI}}{g_{APD}-g_{DI}} \\ 1 \end{pmatrix}. \quad (76)$$

We will assume that  $|g_M - f_{DI} + 1| \ll 1$ , so this mode is stable. If its decay rate is fast enough then its dynamics will be slave to that of the unstable mode, and it will be possible to eliminate it and derive a single amplitude equation for the oscillating mode. In the case in which this mode becomes also unstable (not considered here), then we would have coupled amplitude equations, whose form would depend on the nature of this second instability, i.e., if it is a period doubling or steady bifurcation. A similar situation, with intracellular calcium concentration playing the role of our memory function has been considered in [36]

Since system (72) is not self-adjoint, we have to calculate also the left eigenvalues, that will be necessary in order to derive the amplitude equations. These are:

$$\tilde{v}_l^u = (1, -\frac{f_M}{1 + g_M}), \quad \tilde{v}_l^s = (\frac{g_{APD} - g_{DI}}{1 + g_M}, 1). \quad (77)$$

Then  $\tilde{v}_l^u \cdot v_r^u = \tilde{v}_l^s \cdot v_r^s = 1 + (1 - f_{DI})/(1 + g_M)$ , and  $\tilde{v}_l^u \cdot v_r^s = \tilde{v}_l^s \cdot v_r^u = 0$ .

## B. Amplitude equations

We will assume that there is a critical value of the period  $\tau = \tau_c$  (and corresponding  $APD_c$  and  $M_c$ ) at which condition (74) is satisfied. Then, close to the period doubling bifurcation, we can expand the fields as

$$\begin{pmatrix} APD^{n+1}(x) \\ M^{n+1}(x) \end{pmatrix} = \begin{pmatrix} APD_c \\ M_c \end{pmatrix} + a^n(x)v_r^u + c^n(x)v_r^s, \quad (78)$$

where  $a^n(x)$  and  $c^n(x)$  are the amplitudes of the unstable and stable modes, respectively. Expanding also the period, we finally have

$$T^n = \tau_c - \delta\tau + b^n(x), \quad (79)$$

$$APD^n = APD_c + a^n(x) + \frac{1 - f_{DI}}{g_{APD} - g_{DI}}c^n(x), \quad (80)$$

$$M^n = M_c - a^n(x)\frac{1 - f_{DI}}{f_M} + c^n(x). \quad (81)$$

To obtain the equation for the amplitudes of the modes, we have to introduce these expressions in the maps (69), (70), and then project over the left eigenvalues of the stable and unstable modes. We will also assume the scalings  $c^n \sim \delta\tau \sim (a^n)^2$  and  $b^n \sim (a^n)^3$ , valid for a rapidly decaying stable mode, and small dispersion. Then, for the stable mode we have

$$c^{n+1} = (g_M - f_{DI} + 1)c^n - \delta\tau \frac{g_{DI} + f_{DI}(1 - f_{DI})/f_M}{1 + (1 - f_{DI})/(1 + g_M)} + \omega_1(a^n)^2 + \dots, \quad (82)$$

where  $\omega_1$  is a complicated function of the derivatives of the maps. If the decay rate of  $c^n$  is fast, then we can take the adiabatic approximation, i.e., we consider that  $a^n$  remains almost constant in the time scale for the decay of  $c^n$ . With this approximation we can solve Eq. (82), taking into account that the solution to the difference equation  $c^{n+1} = \alpha c^n + \beta$  is  $c^n = \alpha^n c^0 + \beta(1 - \alpha^n)/(1 - \alpha)$ . Again, if the mode is stable and decays fast enough we can consider  $\alpha^n \rightarrow 0$ , and obtain

$$c^n(x) = \frac{1}{f_{DI} - g_M} \left[ -\delta\tau \frac{g_{DI} + f_{DI}(1 - f_{DI})/f_M}{1 + (1 - f_{DI})/(1 + g_M)} + \omega_1[a^n(x)]^2 \right]. \quad (83)$$

Projecting over the left eigenvector of the unstable mode we obtain an equation for  $a^{n+1}(x)$

$$\begin{aligned} \left(1 + \frac{1 - f_{DI}}{1 + g_M}\right) a^{n+1} = & - \left(1 + \frac{1 - f_{DI}}{1 + g_M}\right) a^n + \left(f_{DI} - g_{DI} \frac{1 - f_{DI}}{g_{APD} - g_{DI}}\right) (b^n - \delta\tau) \\ & + \omega_2(a^n)^2 + \omega_3 a^n c^n + \omega_4(a^n)^3 + w \partial_x a^n - \xi^2 \partial_x^2 a^n + \dots, \end{aligned} \quad (84)$$

where again the coefficients  $\omega_2$ ,  $\omega_3$  and  $\omega_4$  are complicated functions of the derivatives of the maps that we do not write explicitly. Substituting the expression for  $c^n$  in (84), we obtain a single equation for the evolution of  $a^n(x)$ . Since this is the amplitude of an oscillatory mode, it is more useful to consider the equation for the second iteration  $a^{n+2}(x)$ , that evolves slowly in time. Factoring out the rapid oscillations, we can write  $a^n(x) \equiv (-1)^n a(x, t)$ , where we have defined a continuous time through  $t = n\tau_c$ . Then  $a^{n+2} \simeq a^n + 2\tau_c \partial_t a$ . Considering also  $b^n(x) \equiv (-1)^n b(x, t)$ , we obtain the final equation

$$\tau \partial_t a = \sigma \delta \tau a - g a^3 - w \partial_x a + \xi^2 \partial_x^2 a - \beta b, \quad (85)$$

with

$$\tau = \tau_c \left( 1 + \frac{1 - f_{DI}}{1 + g_M} \right) = \tau_c \left[ 1 - f_M \frac{g_{DI} - g_{APD}}{(1 + g_M)^2} \right], \quad (86)$$

$$\beta = 1 - f_M \frac{g_{APD}}{1 + g_M} = f_{DI} - f_M \frac{g_{DI}}{1 + g_M}, \quad (87)$$

and  $\sigma$  and  $g$  some complicated functions that we do not write here. When  $f_M = 0$  we recover the results of the single map.

Assuming that CV-restitution depends only on the diastolic interval, and not on the memory function, so Eq. (9) still holds, the equation for the oscillations in period remains the same

$$\frac{db}{dx} = \frac{a}{\Lambda}. \quad (88)$$

Eqs. (85) and (88) constitute the new set of amplitude equations for this case.

## VI. DISCUSSION

Cardiac alternans are thought to be a key ingredient to explain the transition from ventricular tachycardia (VT) to ventricular fibrillation (VF). VF usually develops from more ordered re-entrant waves (spirals or scroll waves, in two and three dimensional tissue, respectively) which then break down into a turbulent activity. Alternans have been shown to induce spiral break-up [8, 37], leading to a disordered spatio-temporal state that is usually identified with fibrillation. From this work, it has been hypothesized that a restitution curve of slope larger than one is necessary for the transition from VT to VF [8, 37]. Although some experiments support this hypothesis [38], there is so far no conclusive evidence [39].

From a theoretical point of view, and despite earlier progress [8], we still do not have a complete understanding on how alternans affect the stability of spirals. Numerical simulations show that break-up occurs when the amplitude of alternans oscillation grows enough to induce conduction blocks, which typically happens away from the spiral core. However, there is presently no theory that predicts the spatial distribution of alternans in a spiral wave. Topological arguments impose the existence of a nodal line (also termed line defect) [40], with a jump in  $2\pi$  in the phase of the oscillation, stretching from the core of the spiral to the boundaries. Thus, discordant alternans are always present, but what determines the motion of the nodal line, and whether it is important for spiral break-up is not entirely clear, except far from the spiral core where the dynamics is essentially one-dimensional.

In the present paper, we have considered the simpler cases of one and two-dimensional paced tissue and a circulating pulse in a ring geometry, and derived an equation for the spatio-temporal dynamics of small amplitude alternans in these states. Although conduction blocks fall out of the scope of the present theory, since it only considers small variations in conduction velocity, the results do shed light on where conduction blocks will occur. For that one can look at the distribution of *APD* and locate the places where it is larger than a critical value. To study the evolution after a conduction block has occurred, one has to resort again to simulations of the original equations.

A circulating pulse in a ring has long been considered as a simplified model of anatomical reentry [41]. For rings smaller than a critical value, oscillations in *APD* appear [9]. An understanding of these oscillations can be helpful in terminating anatomical reentry circuits. In this case discordant alternans are always present, and their wavelength is determined by the length of the ring, with the fastest growing mode having  $\lambda \simeq 2L$ . In the paced case, it has been shown [3] that the gradients of repolarization created during discordant alternans offer a substrate for conduction block, leading to reentry and ventricular fibrillation. We have shown here that discordant wave patterns [3, 5, 6, 7] result from a finite wavelength linear instability. Hence, their formation requires a minimum tissue size  $L_{min} \sim \lambda/4$ , required for at least one node to form. The value of  $L_{min}$  that we measure in simulations of reaction-diffusion models are actually close to  $\lambda/4$  with  $\lambda$  predicted by Eq. (55) and Eq. (58), respectively (Table I). This lengthscale is similar in two-dimensional paced tissue, although in this case, curvature of the nodal line may affect the motion of this line. In both paced one- and two-dimensional tissue and the ring geometry, the onset of alternans is different in

tissue than in a paced isolated cell because alternans, in tissue, is manifested as a wave and diffusive coupling tends to smooth out spatial gradients of *APD*. An interesting result of our analysis of memory effects is that discordant alternans would not form if the coefficient  $\beta$  in Eq. (85), which depends on the beat-to-beat dynamics, is negative. Therefore, this result opens the possibility to prevent the formation of discordant alternans by altering the beat-to-beat dynamics despite a positively sloped CV-restitution curve.

The paced and reentrant geometries studied in the present paper also form the basis to develop a theory of the dynamics of alternans in the presence of spiral waves, which has been the subject of both experimental and numerical studies [40]. Far from the core, the spiral is similar to the two-dimensional paced case. In the case where nodes move towards the pacing site in a one-dimensional cable, the nodal line should form a spiral with an opposite chirality as the propagating spiral wave front. This opposite chirality is imposed by the fact that the nodal line moves inward towards the core under the effect of a sufficiently steep, positively sloped, CV-restitution curve, and under the assumption that cellular alternans are driven by APD restitution. The wavelength of the nodal line spiral far from the spiral core should be equal to the wavelength of discordant alternans in the one-dimensional paced case. This nodal line should match to the nodal line expected from one-dimensional reentry close to the spiral core. This nodal line should extend straight out of the spiral core in the simplest limit of a constant wave speed where the wavelength of discordant alternans diverges far from the core. A theory for the spiral must, therefore, reduce to the two cases studied in this paper in the appropriate limits. The development of a theory of alternans in this case remains a fascinating task for future work.

## VII. CONCLUSIONS

We have derived an equation that describes the spatio-temporal dynamics of small oscillation alternans in cardiac tissue. Our formulation is based on the restitution properties of the system, and takes also into account intercellular coupling, which is crucial in order to derive the correct threshold pacing rate and lengthscale of discordant alternans. For a simplified two-variable ionic model, we have been able to calculate these coefficients, and show that our reduced description agrees well with numerical simulations of the model. We have also considered the more realistic Noble model, and measured these coefficients numerically,

stressing the generality of our formulation. We have applied our formulation to two different cases, a paced tissue and a circulating pulse in a ring.

In the ring, the amplitude equation predicts that both dispersion and intercellular coupling affect the frequency of the motion, and the oscillations of *APD* are typically quasiperiodic. There is a particular value of the length of the ring where these two effects balance each other, and the oscillations become periodic. For the paced case, the amplitude equation predicts that discordant wave patterns result from a finite wavelength linear instability. Hence, their formation requires a minimum tissue size  $L_{min} \sim \lambda/4$ , required for at least one node to form. It should be emphasized that this lengthscale is intrinsic, in opposition to the circulating pulse, where it depends on the length of the ring. From the linear problem we deduce the possibility of two different patterns, depending on the parameters of the system, a standing wave pattern, or a traveling one. In the latter state, the amplitude of the oscillation grows exponentially away from the pacing point in a linear regime, which favors the induction of conduction blocks.

Even though the present theory does not take into account several effects present in real tissue (such as the three dimensional fiber geometry of an anatomical heart, the corresponding anisotropy in conduction velocity, spatial gradients of restitution properties, etc) it sheds light on the basic mechanisms and length scales that control the formation and evolution of discordant alternans. Moreover, it identifies a small subset of relevant parameters that control the formation of these arrhythmogenic patterns in experiments and numerical simulations of more complex ionic models.

### Acknowledgments

This work was supported by National Institutes of Health/National Heart, Lung, and Blood Institute Grants P50-HL52319 and P01 HL078931. B.E. wants to acknowledge financial support by MCyT (Spain), and by MEC (Spain), under project FIS2005-06912-C02-01.

### APPENDIX A: DERIVATION OF THE KERNEL

Let us show how to calculate the kernel in Eq. (10), and the coefficients  $w$  and  $\xi^2$ , for the two-variable model. This will allow us to verify the theory, as we can compare our

analytical results with the simulations, and also gain some physical intuition on the origin of these coefficients. To explain which is the origin of the kernel we have to go back to the cable equation (3) (with  $I_{ext} = 0$ ). We want to know what effect does a gradient of  $APD$  have on the restitution curve. For that, we will consider a single pulse propagating in this gradient with speed  $c$ . Interpreting the cable equation as a diffusion equation where  $I_{ion}$  is a spatially distributed source, Eq. (3) can be formally inverted, expressing the transmembrane potential  $V$  in terms of the Green function of the diffusion operator:

$$V(x, t) = \frac{1}{C_m} \int_{-\infty}^t dt' \int_{-\infty}^{\infty} dx' \frac{\exp\left\{-\frac{(x-x')^2}{4D(t-t')}\right\}}{[4\pi D(t-t')]^{1/2}} I_{ion}(x', t'), \quad (A1)$$

where we have assumed translational invariance, as is the case in the ring.

Now, if we are measuring the action potential duration at a given value of the transmembrane potential  $V_c$ , then, by definition

$$V_c = V(x, x/c + A(x)), \quad (A2)$$

where  $x/c$  is the time it took the pulse to arrive at position  $x$  and, for simplicity we introduce the notation  $A(x) \equiv APD(x)$ . Substituting this into Eq. (A1), we obtain

$$V_c = \frac{1}{C_m} \int_{-\infty}^{x/c+A(x)} dt' \int_{-\infty}^{\infty} dx' \frac{\exp\left\{-\frac{(x-x')^2}{4D(x/c+A(x)-t')}\right\}}{[4\pi D(x/c+A(x)-t')]^{1/2}} I_{ion}(x', t'). \quad (A3)$$

This defines an implicit integral equation for the action potential duration.

In the general case it is not clear how to invert this equation. We can do it, however, for the simpler case of the two variable model, where the action potential adopts a triangular form. Integrating Eq. (5) for the gate variable  $h$  (in the limit  $\epsilon \rightarrow 0$ ), for  $V > V_c$ , we obtain  $h = h_0 e^{-t/\tau_+}$ , where  $h_0 = 1 - e^{-DI/\tau_-}$  can be obtained integrating Eq. (5) for  $V < V_c$ , and assuming  $\tau_+ \ll \tau_-$ , so by the time of pacing ( $t = DI$ ) the gate is completely closed ( $h = 0$ ).

Then, when  $V > V_c$ , and in the absence of propagation, the equation for the temporal evolution of the transmembrane potential becomes (assuming  $t = 0$  when  $V = V_c$ ):

$$\dot{V} = \frac{1}{\tau_a} (1 - e^{-DI/\tau_-}) e^{-t/\tau_+} - \frac{1}{\tau_0}. \quad (A4)$$

When  $\tau_+ \ll \tau_0$  we can assume that depolarization occurs instantaneously, so we can write the current in the form

$$I_{ion}(t)/C_m = -\theta(t)I + \delta(t)J[DI], \quad (A5)$$

where  $\theta(t)$  is the step function, and  $\delta(t)$  the Dirac delta function. The former equation means that, after an excitation at  $t = 0$ , the voltage takes the maximum value  $V_{max} = J[DI]$  and then decreases linearly in time  $V = V_{max} - It$ , with the identifications  $J[DI] = \tau_+(1 - e^{-DI/\tau_-})/\tau_a$  and  $I = 1/\tau_0$ .

Integrating Eq. (A4) we obtain

$$V(t) = \frac{\tau_+}{\tau_a}(1 - e^{-DI/\tau_-})(1 - e^{-t/\tau_+}) - \frac{t}{\tau_0} = V_{max}(1 - e^{-t/\tau_+}) - \frac{t}{\tau_0}. \quad (\text{A6})$$

Again assuming that  $\tau_+ \ll \tau_0$ , the value of the *APD* becomes  $APD = (V_{max} - V_c)\tau_0$ , or

$$APD^{n+1} = (J[DI^n] - V_c)/I \equiv f(DI^n), \quad (\text{A7})$$

which gives us the APD-restitution.

For a propagating pulse in a gradient of DI, we can again use expression (A5), but taking into account that the excitation now occurs when the pulse arrives (i.e. at time  $t = x/c$ ), and that the diastolic interval depends on space. Then

$$I_{ion}(x, t)/C_m = -\theta(t - x/c)I + \delta(t - x/c)J[DI(x)]. \quad (\text{A8})$$

Substituting this expression into (A3) we can now split the integral into two parts  $V_c = V_I + V_{II}$ . The first part is

$$\begin{aligned} V_I &= \int_{-\infty}^{x/c+A(x)} dt' \int_{-\infty}^{\infty} dx' \frac{\exp\left\{-\frac{(x-x')^2}{4D(x/c+A(x)-t')}\right\}}{[4\pi D(x/c+A(x)-t')]^{1/2}} \theta(t' - x'/c)I \\ &= I \int_{-\infty}^{x/c+A(x)} dt' \int_{-\infty}^{ct'} dx' \frac{\exp\left\{-\frac{(x-x')^2}{4D(x/c+A(x)-t')}\right\}}{[4\pi D(x/c+A(x)-t')]^{1/2}}. \end{aligned} \quad (\text{A9})$$

This gives

$$V_I = I \int_{-\infty}^{x/c+A(x)} dt' \frac{1}{2} \left\{ 1 + \text{Erf} \left[ \frac{ct' - x}{\sqrt{4D(x/c+A(x)-t')}} \right] \right\}. \quad (\text{A10})$$

Making the approximation

$$\frac{1}{2} \left\{ 1 + \text{Erf} \left[ \frac{y}{\sqrt{4D(A(x) - y/c)}} \right] \right\} \simeq \theta(y), \quad (\text{A11})$$

valid when  $D/c \ll (DA)^{1/2} \ll Ac$ , we obtain

$$V_I \simeq I \int_{-\infty}^{x/c+A(x)} dt' \theta(ct' - x) = IA(x). \quad (\text{A12})$$

As long as the length scales associated with intercellular coupling are small compared with the distance the pulse travels during an *APD* (so the coupling with other cells is negligible), this integral gives us the change in voltage during repolarization at a given point, during the time of one *APD*.

The other integral is

$$\begin{aligned} V_{II} &= \int_{-\infty}^{x/c+A(x)} dt' \int_{-\infty}^{\infty} dx' \frac{\exp\left\{-\frac{(x-x')^2}{4D(x/c+A(x)-t')}\right\}}{[4\pi D(x/c+A(x)-t')]^{1/2}} J[D(x')] \delta(t' - x'/c) \\ &= \int_{-\infty}^{x/c+A(x)} dt' \frac{\exp\left\{-\frac{(x-ct')^2}{4D(x/c+A(x)-t')}\right\}}{[4\pi D(x/c+A(x)-t')]^{1/2}} c J[D(ct')]. \end{aligned} \quad (\text{A13})$$

Making the change of variable  $t' = (x + y)/c$ , we finally obtain

$$V_{II} = \int_{-\infty}^{cA(x)} dy \frac{\exp\left\{-\frac{y^2}{4D(A(x)-y/c)}\right\}}{[4\pi D(A(x)-y/c)]^{1/2}} J[D(x+y)]. \quad (\text{A14})$$

And this integral gives us the correction to the maximum value of the *APD* coming from the intercellular coupling, as  $V_{II} \simeq V_{max}$ .

Adding the two terms, and solving for  $A(x)$  in Eq. (A12), we obtain

$$\begin{aligned} A(x) &= \int_{-\infty}^{\infty} dy \frac{\exp\left\{-\frac{y^2}{4D(A(x)-y/c)}\right\}}{[4\pi D(A(x)-y/c)]^{1/2}} (J[DI(x+y)] - V_c)/I \\ &\equiv \int_{-\infty}^{\infty} dy \frac{\exp\left\{-\frac{y^2}{4D(A(x)-y/c)}\right\}}{[4\pi D(A(x)-y/c)]^{1/2}} f[DI(x+y)], \end{aligned} \quad (\text{A15})$$

where  $A(x)$  is the *APD* following the diastolic interval  $DI$ , so  $A(x) \equiv APD^{n+1}$  and  $DI \equiv DI^n$ , and we have extended the limits of the integral to infinity, assuming a rapid decay of the kernel. It should be noticed that  $A(x)$  is still in the kernel, so the former equation gives an implicit expression for the *APD*. As we are interested in the regime close to the onset of period doubling, we can approximate the *APD* within the integral as  $A(x) \simeq A_c$ . The deviations from the critical value would give nonlinear gradient terms in the oscillations of *APD*, that we assume to be of higher order. Then, our final expression is:

$$APD^{n+1}(x) = \int_{-\infty}^{\infty} dy \frac{\exp\left\{-\frac{y^2}{4D(A_c-y/c)}\right\}}{[4\pi D(A_c-y/c)]^{1/2}} f[DI^n(x+y)]. \quad (\text{A16})$$

Once we know the expression for the kernel, the coefficients  $w$  and  $\xi^2$  are easy to obtain. It is useful to rewrite the kernel using the change of variable  $y = 2(D A_c)^{1/2} z$ . Then, expanding the kernel to first order in the coefficient  $2(D A_c)^{1/2}/(A_c c)$ , again assumed to be small, we

get

$$APD^{n+1}(x) = \frac{1}{\sqrt{\pi}} \int_{-\infty}^{\infty} dz e^{-z^2} [1 + \frac{1}{c} \sqrt{\frac{D}{A_c}} (z - 2z^3)] f[DI^n(x + 2(DA_c)^{1/2}z)]. \quad (\text{A17})$$

We can expand the restitution curve around its value at a given point

$$\begin{aligned} f[DI^n(x + y)] &= f \left[ DI^n(x) + y \partial_x DI^n(x) + \frac{1}{2} y^2 \partial_x^2 DI^n(x) + \dots \right] \\ &= f[DI^n(x)] + 2z(DA_c)^{1/2} f' \partial_x DI^n(x) + 2z^2 DA_c f' \partial_x^2 DI^n(x) + \dots \end{aligned} \quad (\text{A18})$$

Introducing this in Eq. (A17), the asymmetrical part results

$$\frac{2D}{c} f' \partial_x DI^n(x) \frac{1}{\sqrt{\pi}} \int_{-\infty}^{\infty} dz e^{-z^2} (z^2 - 2z^4) = -\frac{2D}{c} f' \partial_x DI^n(x), \quad (\text{A19})$$

and the symmetrical one

$$2DA_c f' \partial_x^2 DI^n(x) \sqrt{\pi} \int_{-\infty}^{\infty} dz e^{-z^2} z^2 = DA_c f' \partial_x^2 DI^n(x). \quad (\text{A20})$$

Therefore, we have

$$APD^{n+1}(x) = f[DI^n(x)] - \frac{2D}{c} f' \partial_x DI^n(x) + DA_c f' \partial_x^2 DI^n(x) + \dots \quad (\text{A21})$$

This expression is the same as Eq. (37). Identifying terms we obtain the values  $w = 2D/c$ ,  $\xi^2 = DA_c$ . For more complicated ionic models these coefficients have to be calculated numerically.

- [1] T. Lweis, Q. J. Med. **4**, 141 (1910).
- [2] P.J. Schwartz, A. Malliani, Am. Heart J. **89**, 45 (1975); J.M. Smith, E.A. Clancy, R. Valeri, J. N. Ruskin, R.J. Cohen, Circulation **77**, 110 (1988); B. Nearing, A. H. Huang, and R. L. Verrier, Science **252**, 437 (1991); D. S. Rosenbaum, L. E. Jakson, J. M. Smith, H. Garam, J. N. Ruskin, R. J. Cohen, N. Engl. J. Med. **330**, 235 (1994).
- [3] J. M. Pastore, S. D. Girouard, K. R. Laurita, F. G. Akar and D. S. Rosenbaum, Circulation **99**, 1385 (1999).
- [4] G. R. Mines, J. Physiol. (Lond.) **46**, 349 (1913).
- [5] J. J. Fox, M. L. Riccio, F. Hua, E. Bodenschatz, and R. F. Gilmour, Circulation Research **90**, 289 (2002).

[6] Z. Qu , A. Garfinkel, P-S. Chen, J. W. Weiss, *Circulation* **102**, 1664 (2000).

[7] M. A. Watanabe , F. H. Fenton, S. J. Evans, H. M. Hastings and A. Karma, *J. Cardiovasc. Electrophys.* **12**, 196 (2001).

[8] A. Karma, *Chaos* **4**, 461 (1994).

[9] L.H. Frame and M.B. Simson, *Circulation* **78**, 1277 (1988).

[10] M. Courtemanche, L. Glass, and J. P. Keener, *Phys. Rev. Lett.* **70**, 2182 (1993); M. Courtemanche, J. P. Keener, and L. Glass, *SIAM J. Appl. Math.* **56**, 119 (1996).

[11] A. Vinet, *Annals Biomed. Eng.* **28**, 704 (2000).

[12] D. S. Rosenbaum, *J. Cardiovasc. Electrophys.* **12**, 207 (2001).

[13] K. R. Laurita, S. D. Girouard, and D. S. Rosenbaum, *Circulation Research* **79**, 493 (1996).

[14] J. N. Weiss, A. Karma, Y. Shiferaw, P. S. Chen, A. Garfinkel, Z. Qu, *Circ. Res.* **98**, 1244 (2006).

[15] J. B. Nolasco and R. W. Dahlen, *J. App. Physiol.* **25**, 191 (1968).

[16] M. R. Guevara , G. Ward, A. Shrier, and L. Glass in *Computers in Cardiology*, IEEE Comp. Soc., pp. 167 (1984).

[17] F. H. Fenton, S. J. Evans, and H. M. Hastings, *Phys. Rev. Lett.* **83**, 3964 (1999).

[18] G.M. Hall, S. Bahar, and D.J. Gauthier, *Phys. Rev. Lett.* **82**, 2995 (1999).

[19] J.J. Fox, E. Bodenschatz, and R.F. Gilmour, *Phys. Rev. Lett.* **89**, 138101 (2002).

[20] Y. Shiferaw, M. watanabe, A. Garfinkel, J. Weiss, and A. Karma, *Biophys. J.* **85**, 3666 (2003).

[21] Y. Shiferaw, D. Sato, and A. Karma, *Physical Review E* **71**, 021903 (2005).

[22] B. Echebarria and A. Karma, *Phys. Rev. Lett.* **88**, 208101 (2002).

[23] B. Echebarria and A. Karma, *Chaos* **12**, 923 (2002).

[24] D. J. Christini, M. L. Riccio, C. A. Culianu, J. J. Fox, A. Karma, and R. F. Gilmour Jr., *Phys. Rev. Lett.* **96**, 104101 (2006).

[25] M. C. Cross and P. C. Hohenberg, *Rev. Mod. Phys.* **65**, 851 (1993).

[26] D. Noble, *J. Physiol* **160**, 317 (1962).

[27] E. Cytrynbaum and J. P. Keener, *CHAOS* **12**, 788 (2002).

[28] E.G. Tolkacheva, D.G. Schaeffer, D.J. Gauthier, and W. Krassowska, *Phys. Rev. E* **67**, 031904 (2003).

[29] Eq. (40) becomes, in the case of the Noble model:  $\tau \partial_t a = \sigma a - ga^3 - \chi a^5 - b - w \partial_x a + \xi^2 \partial_x^2 a$ , with the coefficients  $\sigma = 5.71 \cdot 10^{-3}(\tau_c - \tau)$ ,  $g \simeq -8 \cdot 10^{-6}$ , and  $\chi \simeq 1.37 \cdot 10^{-8}$ . For the two-variable

model we have used the analytical form of the *APD*-restitution curve, given by Eq. (6), so the coefficients are  $\sigma = (\tau_c - \tau)/(2\tau_-) = 8.33 \cdot 10^{-3}(\tau_c - \tau)$  and  $g = 1/(12\tau_-^2) = 2.31 \cdot 10^{-5}$ .

- [30] K. L. Babcock, G. Ahlers, and D. S. Cannell, Phys. Rev. Lett. **67**, 3388 (1991).
- [31] S.M. Tobias, M.R.E. Proctor, and E. Knobloch, Physics D, **113**, 43 (1998).
- [32] J.J. Fox, R.F. Gilmour, and E. Bodenschatz, Phys. Rev. Lett. **89**, 198101-1 (2002).
- [33] H. Henry and W.-J. Rappel, Phys. Rev. E **71**, 051911 (2005).
- [34] P. Comtois, A. Vinet, and S. Nattel, Phys. Rev. E **72**, 031919 (2005).
- [35] D.R. Chialvo, D.C. Michaels, and J. Jalife, Circ. Res. **66**, 525 (1990).
- [36] Y. Shiferaw and A. Karma, PNAS **103**, 5670 (2006)
- [37] M. Courtemanche, Chaos **6**, 579 (1996); J.N. Weiss, A. Garfinkel, H.S. Karaguezian, Z. Qu, and P.S. Chen, Circulation **99**, 2819 (1999).
- [38] M. L. Riccio, M. L. Koller, and R. F. Gilmour, Circ. Res. **84**, 955 (1999); A. Garfinkel, Y. Kim, O. Voroshilovsky, Z. Qu, J.R. Kil, M-Y. Lee, H.S. Karaguezian, J.N. Weiss, and P-S. Chen, Proc. Natl. Acad. Sci USA **97**, 6061 (2000).
- [39] R.F. Gilmour, N.F. Otani, and M.A. Watanabe, Am. J. Physiol. **272**, H1826 (1997).
- [40] A. Goryachev and R. Kapral, Phys. Rev. E **54**, 5469 (1996); A. Goryachev, H. Chaté, and R. Kapral, Phys. Rev. Lett. **80**, 873 (1998); J-S. Park and K.J. Lee, Phys. Rev. Lett. **83**, 5393 (1999); J.-S. Park, S. J. Woo, and K. J. Lee, Phys. Rev. Lett. **93**, 098302 (2004); S. M. Hwang, T. Y. Kim, and K. J. Lee, Proc. Natl. Acad. Sci. (USA) **102**, 10363 (2005).
- [41] G.R. Mines, Trans. Roy. Soc. Can. **4**, 43 (1914).

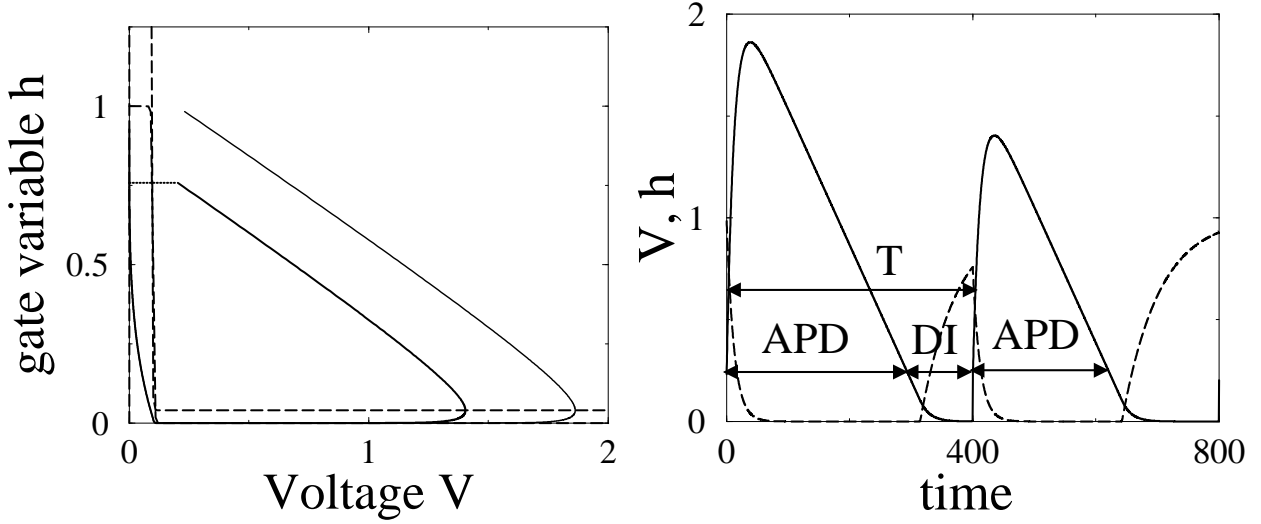


FIG. 1: a) Trajectories in the phase plane ( $V$ ,  $h$ ) for the two-variable model (Eqs. (4)-(5)), obtained simulating  $\dot{V} = -I_{ion}/C_m$ , and giving an stimulus every  $\tau = 400ms$ . The dashed lines denote the nullclines  $h = 0$  and  $V = 0$ . b) Time evolution of the voltage  $V$  (solid line) and the gate variable  $h$  (dashed line) during such trajectory.

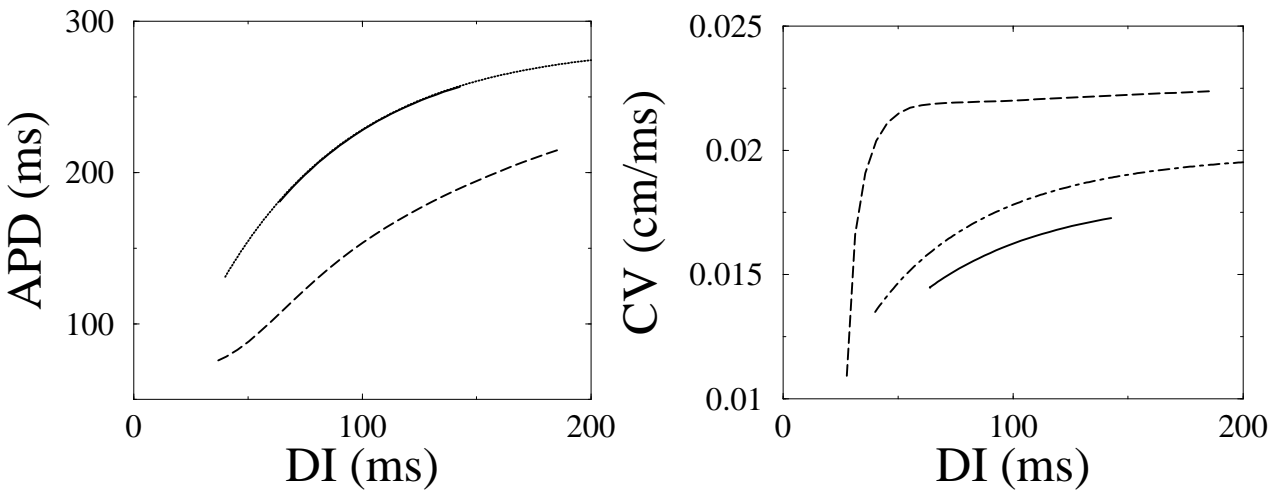


FIG. 2: APD- and CV-restitution curves corresponding to the Noble (long-dashed lines) and two-variable models (solid lines). The dot-dashed line in the right figure corresponds to the approximate expression given by Eq. (8). For the APD the curve obtained from Eq. (6) is indistinguishable from that computed numerically.

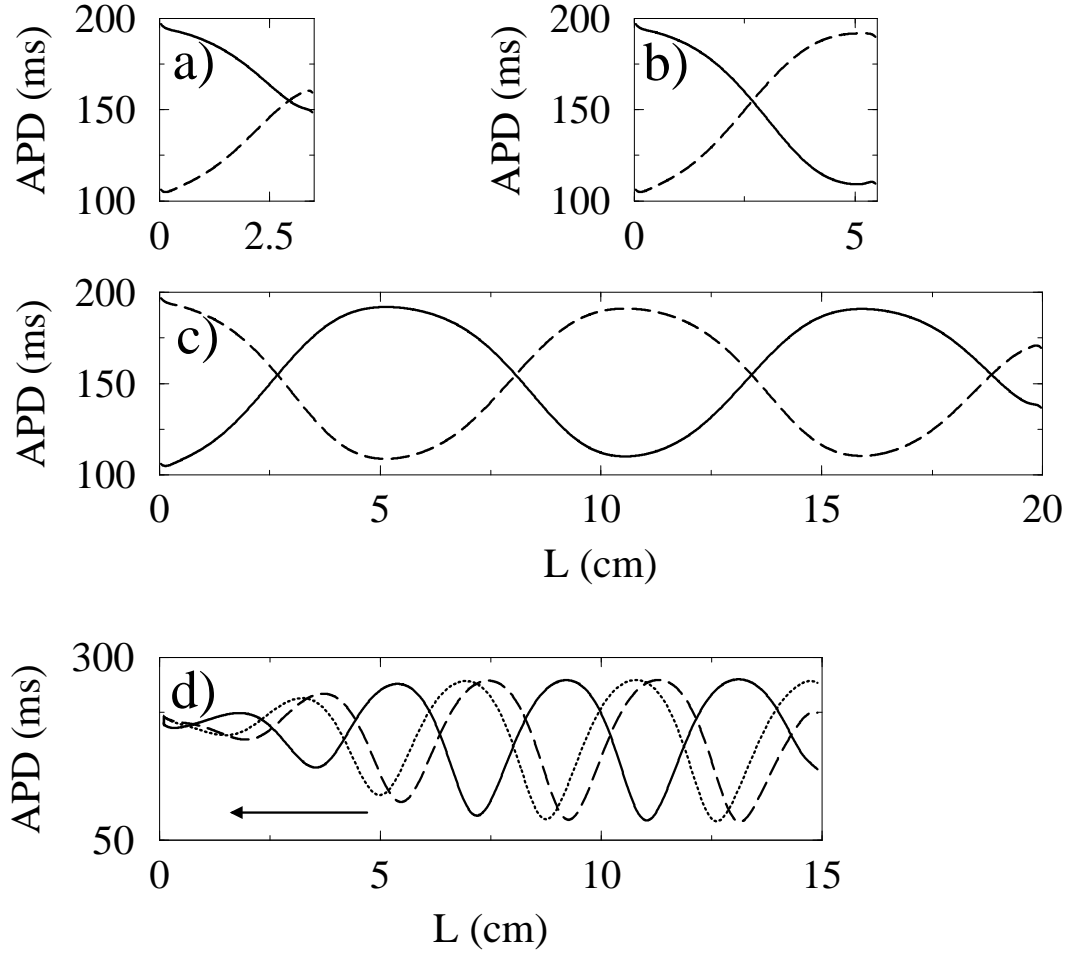


FIG. 3: Distribution of the action potential duration in a long strand of tissue obtained simulating Eq. (3) for the Noble a), b), and c) and two-variable models, d), with  $\tau = 258\text{ms}$ , and  $\tau = 290\text{ms}$ , respectively, and several tissue lengths. The solid and dashed lines correspond to two consecutive beats, while the dotted line in d) represents the APD ten beats later. Thus, in d) the pattern is traveling towards the pacing point.

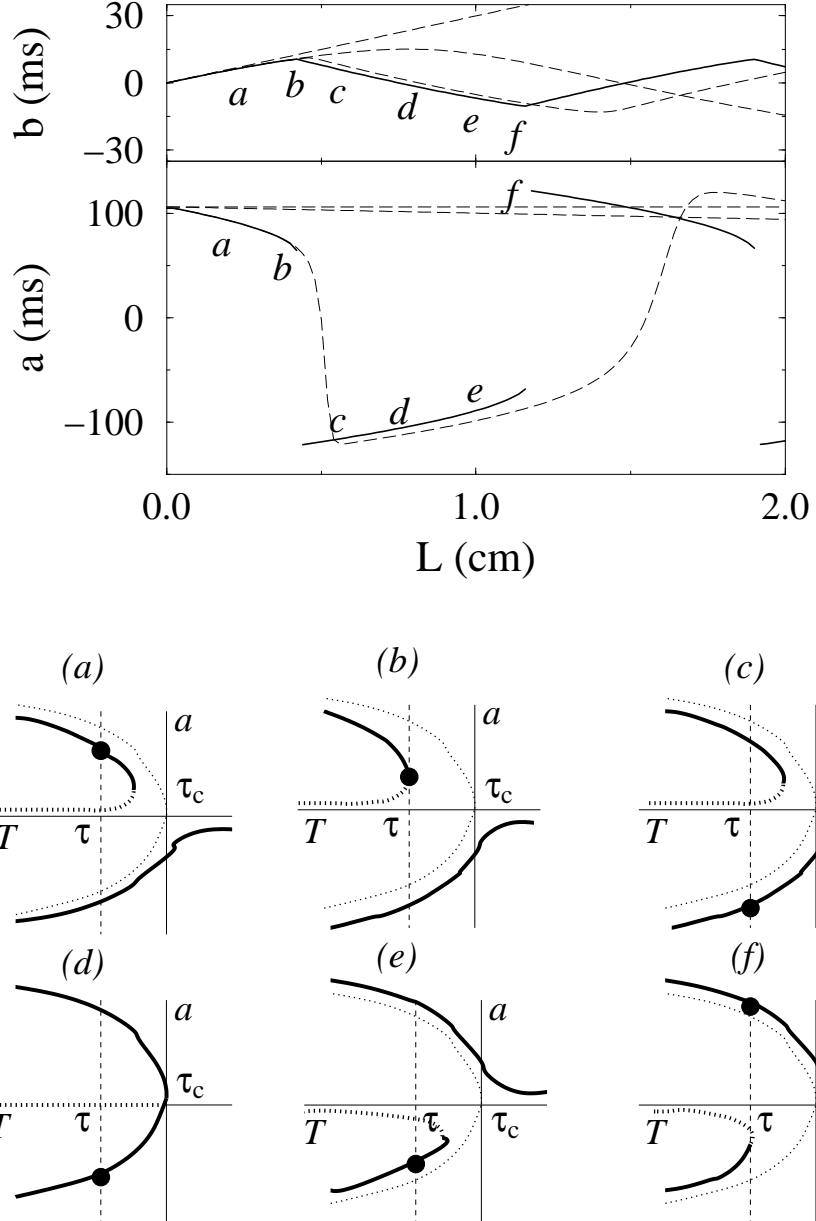


FIG. 4: Upper panel: Oscillations in action potential duration and period, obtained simulating Eqs. (48) and (50), with the parameters of the two-variable model, and  $\tau = 290\text{ms}$ . Starting with a constant value of  $a$ , we show in dashed lines the evolution of the system at times  $t = 0, 10\tau, 50\tau$ , and  $500\tau$ . The final state is shown in solid lines. Below we sketch the bifurcation diagram at several points along the cable for this final state. The dashed line denotes the value of  $T(0) = \tau$  and the filled circle the value of the amplitude of oscillation in *APD* in each case. As we go along the tissue  $b$  becomes positive and the pitchfork (dotted line) becomes and imperfect bifurcation (cf. Eq. (50)) (a). At point (b) the saddle-node is at  $T = T(0)$ . There is a jump to the other phase and  $b$  starts to decrease (c). At (d)  $b = 0$  and a perfect pitchfork bifurcation is recovered, after which the branches switch place (e). Finally, the saddle-node reaches  $T = T(0)$  and the process starts again.

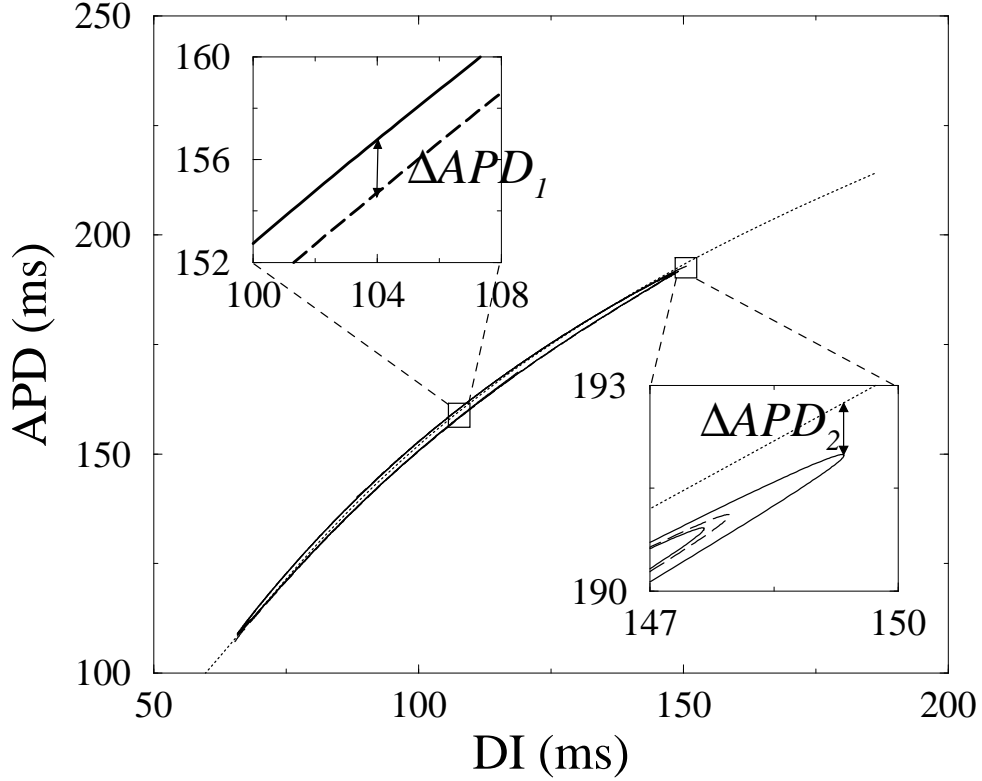


FIG. 5: Restitution curves. The dotted line corresponds to that obtained using a S1S2 protocol, while the solid and dashed lines are the dynamic restitution curves corresponding to the two beats in Fig. 3c. The difference between these two latter curves, at  $APD = APD_c$ ,  $\Delta APD_1$ , gives the change in  $APD$  corresponding to a negative or positive slope. The value  $\Delta APD_2$  is obtained as the difference between the maximum value of the  $APD$  in the dynamic restitution curve (corresponding to Fig 3c), and the value of  $APD$  for the same  $DI$  obtained using a S1S2 protocol, where no gradients are present.

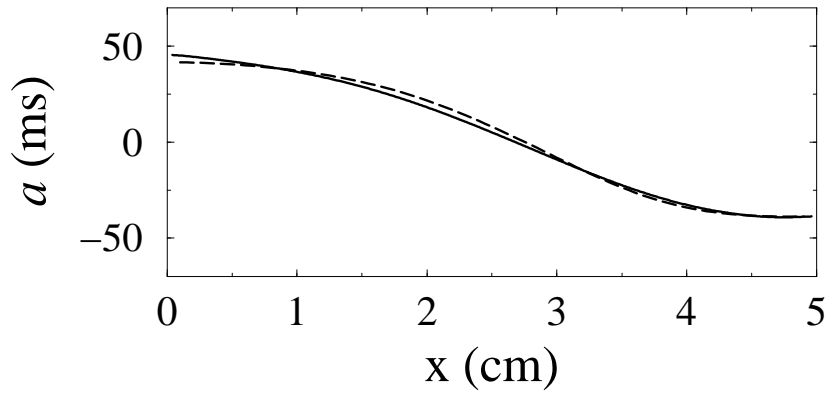


FIG. 6: Comparison of the results obtained simulating the Noble model (solid line) and the amplitude equation (49) (dashed line), with the coefficients given in Table I.

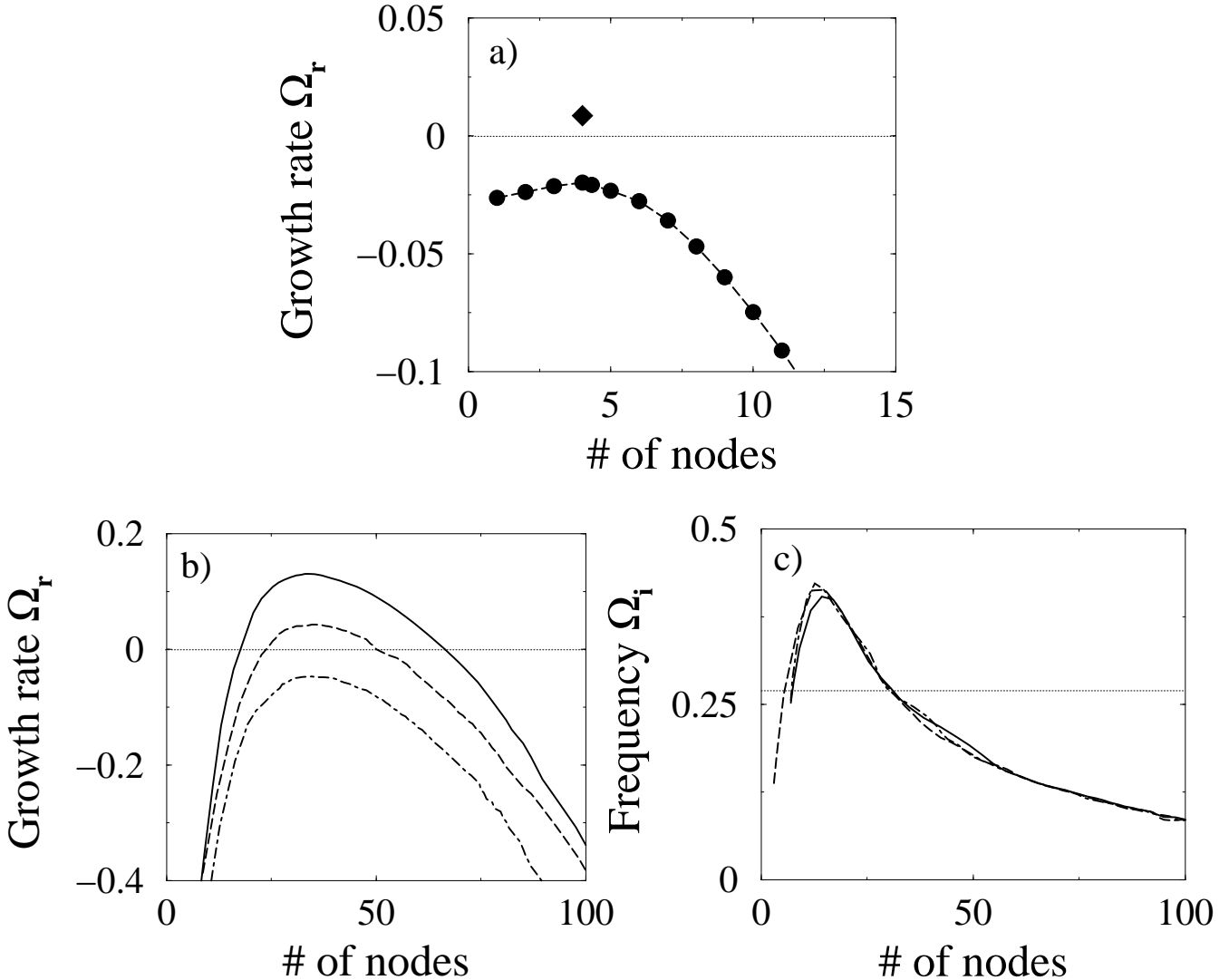
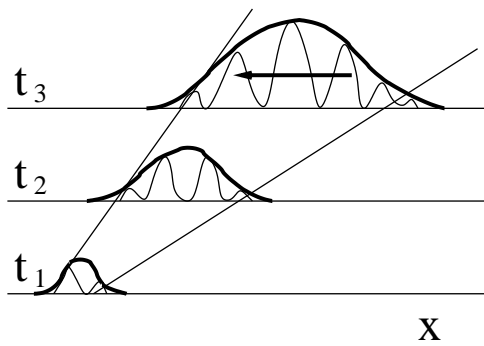


FIG. 7: Results of the linear stability analysis, obtained solving Eq. (53). a) Growth rate vs. number of nodes for the parameters in the Noble model, for  $L = 20\text{cm}$  and  $\tau = 258\text{ms}$ . The spectrum consists of a stable set of eigenvalues plus an isolated unstable mode with four nodes, as expected from Fig. 5. b) Growth rate and c) frequency of the traveling pattern vs. number of nodes, for  $L = 100\text{cm}$ , and the parameters of the two-variable model. In this case there is a band of complex modes that becomes unstable as the pacing period is decreased from  $\tau = 310\text{ms}$  (dot-dashed line) to  $\tau = 300\text{ms}$  (dashed line) and  $\tau = 290\text{ms}$  (solid line). In c) the dotted line represents the value of the frequency given by  $\Omega_i = (3\sqrt{3}/2)(\xi/2\Lambda)^{2/3} \simeq 0.27$ , valid when  $w = 0$ .

a) Convective



b) Absolute

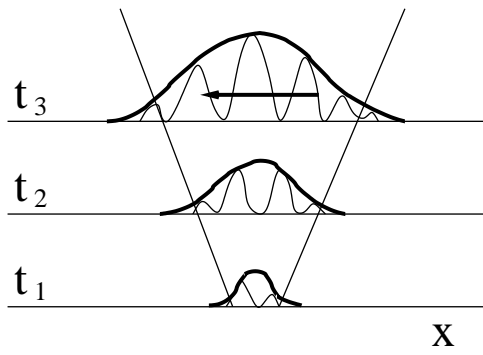


FIG. 8: Convective *vs* absolute instability. When the instability is convective (as in a)), an initial localized perturbation is advected as it grows (here  $t_3 > t_2 > t_1$ ), so at a given point in space it decays. The instability becomes absolute when the wavepacket grows at any given point in space (b). This is signaled by a vanishing group velocity. It should be noted that the phase velocity, however, does not vanish and, in general, it does not have to be in the same direction as the group velocity.

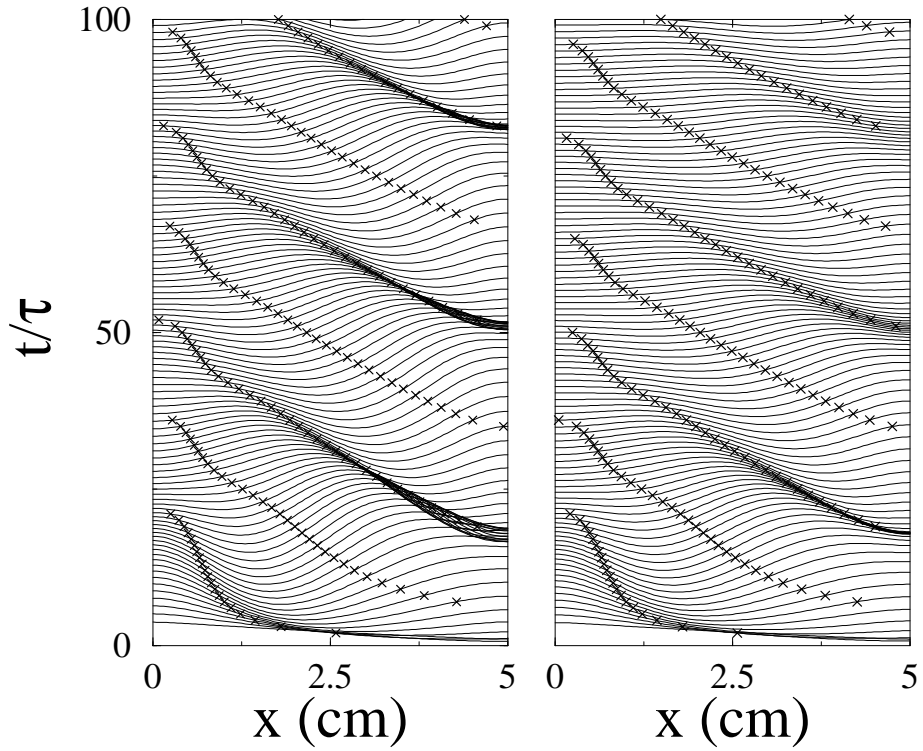


FIG. 9: Space-time plots of  $a$  obtained by simulations of Eq. (49) for parameters of the two-variable model, showing absolutely unstable (left and  $\tau = 295$  ms) and convectively unstable (right and  $\tau = 298$  ms) wave patterns. The crosses denote the positions of the nodes ( $a = 0$ ).

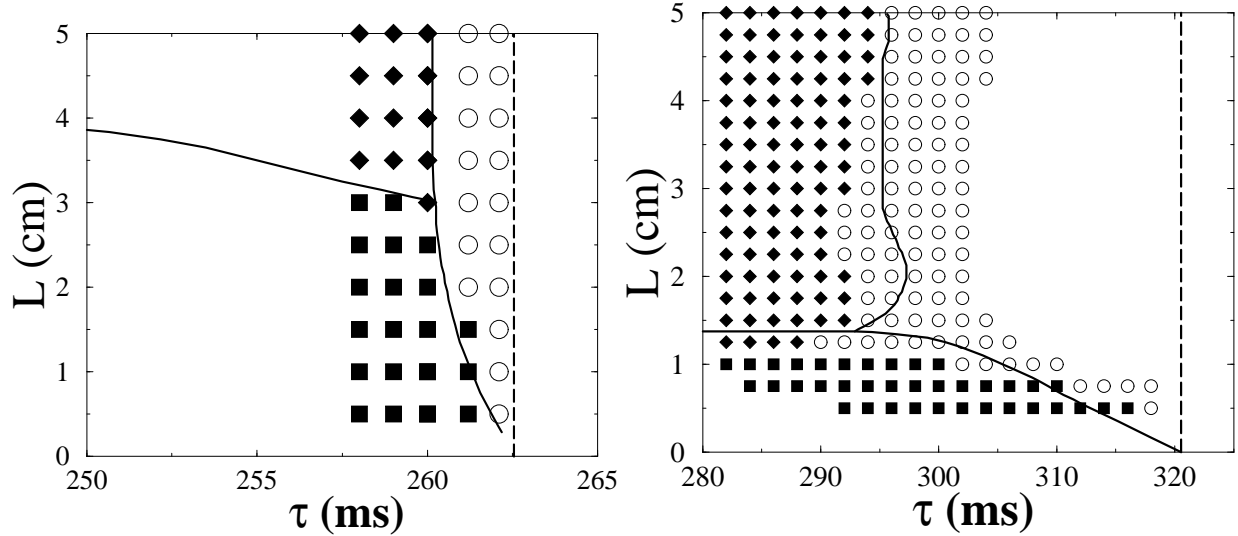


FIG. 10: Stability diagram of the Noble (left panel) and two-variable (right panel) cable models with domains of no-alternans (open circles), concordant alternans (filled squares), and discordant alternans (filled diamonds); conduction blocks form at smaller  $\tau$  not shown here. Boundaries between the same domains obtained by simulations of the amplitude equation (49) are shown by solid lines. The dashed line denotes the bifurcation period for alternans predicted by the map of Eq. (1).

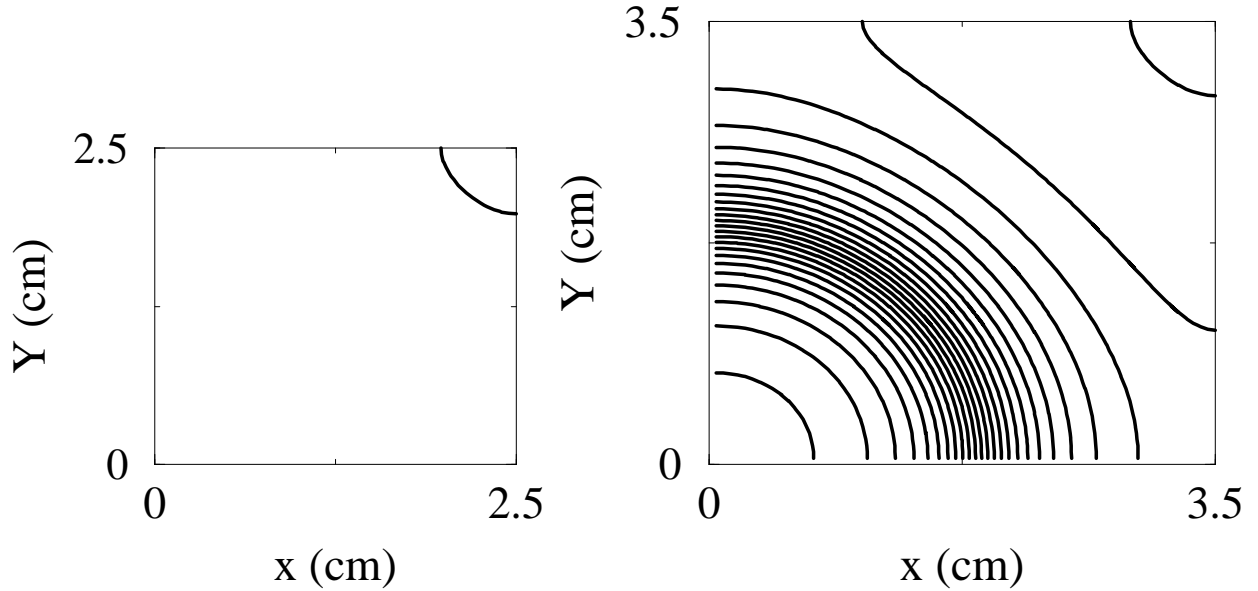


FIG. 11: Simulations of Eq. (67) for the parameters of the Noble model, with  $T_0 = 258$  and a)  $L = 2.5\text{cm}$ , b)  $L = 3.5\text{cm}$ . The solid lines represent the position of the node. The lines in b) are drawn every ten beats. As the size of the tissue increases, a node forms at the corner opposite the pacing point (a), which above a certain tissue size begins to travel, due to curvature effects (b).